Heliyon 9 (2023) e14447

Contents lists available at ScienceDirect

Heliyon

journal homepage: www.cell.com/heliyon

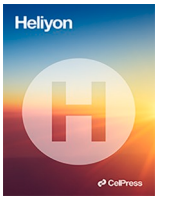

Research article

Self-sustained chaotic floating of a liquid crystal elastomer balloon under steady illumination

Peibao Xu, Haiyang Wu, Yuntong Dai, Kai Li *

Department of Civil Engineering, Anhui Jianzhu University, Hefei, Anhui 230601, PR China

ARTICLE INFO

Keywords:
Self-sustained oscillation
Chaos
Light-powered
Liquid crystal elastomer
Balloon
Floating

ABSTRACT

Self-sustained chaotic system has the capability to maintain its own motion through directly absorbing energy from the steady external environment, showing extensive application potential in energy harvesters, self-cleaning, biomimetic robots, encrypted communication and other fields. In this paper, a novel light-powered chaotic self-floating system is proposed by virtue of a nonlinear spring and a liquid crystal elastomer (LCE) balloon, which is capable of self-floating under steady illumination due to self-beating. The corresponding theoretical model is formulated by combining dynamic LCE model and Newtonian dynamics. Numerical calculations show that the periodic self-floating of LCE balloon can occur under steady illumination, which is attributed to the light-powered self-beating of LCE balloon with shading coating. Furthermore, the chaotic self-floating is presented to be developed from the periodic self-floating through period doubling bifurcation. In addition, the effects of system parameters on the self-floating behaviors of the system are also investigated. The detailed calculations demonstrate that the regime of self-floating LCE balloon depends on a combination of system parameters. The chaotic self-floating system of current study may inspire the design of other chaotic self-sustained motion based on stimuli-responsive materials, and have guiding significance for energy harvesters, self-cleaning, biomimetic robots, encrypted communication and other applications.

1. Introduction

Self-sustained motion refers to a system maintaining its own motion in the presence of energy input from a steady external environment [1–4]. Generally speaking, a self-sustained motion system obtains energy from the external environment to compensate for the damping dissipation during system motion [5–7]. Self-sustained motion generally has strong robustness, with frequency and amplitude depending on system parameters [8–12]. The self-control of self-sustained motion is conducive to the design of complex controllers [13], which has important application prospects in many fields, such as the mobile robots [14,15], active instruments [16–19], energy harvesters [20–23], motors [24], autonomous separation and stirrer [25,26], sensors [27] and biomimetics [28], etc. In addition, the study of self-sustained motion contributes to a deeper understanding of non-equilibrium thermodynamic processes [29,30].

Substantial work has been done to construct a variety of self-sustained motion systems based on active materials, such as liquid crystal elastomers (LCEs) [31–34], hydrogels [35,36], polyelectrolyte gels [37,38] and so on. These active materials are responsive to different external excitations, such as light [6], heat [39], electric field [40] and magnetic field [41], etc., typically exhibiting changes

* Corresponding author.
E-mail address: kli@ahjzu.edu.cn (K. Li).

https://doi.org/10.1016/j.heliyon.2023.e14447
Received 18 October 2022; Received in revised form 2 March 2023; Accepted 7 March 2023
Available online 10 March 2023

in shape and motion state. Through these stimuli-responsive materials, various self-sustained motion modes have been introduced, such as swing [42], rolling [43], rotation [44], bending [45], bouncing [46–48], twisting [49], vibration [50,51] and swimming [52]. These motion modes are originated from different specific mechanisms to maintain the system's own motion, for example, self-shading mechanism [53,54], coupling mechanism between liquid volatilization and membrane deformation [30], and a combination of finite deformation and chemical reaction [37,38]. They absorb energy continuously from the environment through responsive deformation and movement of the material under external excitation, which makes up for the energy dissipated by system damping.

At present, most of the constructed self-sustained motion modes are periodic. Recently, the chaotic self-sustained motion based on active materials has become an object of considerable attention [55]. Kumar experimentally constructed a self-sustained chaotic actuator based on LCE film [55]. This chaotic actuator doped with light-responsive azobenzene enables the polymer film to move under steady illumination [56,57]. With the change of light intensity and wavelength, the motion mode of the LCE film can change significantly. Conventional chaotic systems are mostly mechanical systems that passively acquire energy to compensate for the energy dissipation of system damping [58]. The self-sustained chaotic system of active materials can actively obtain the energy of the external system, which is more in line with the movement form of organisms, and can simulate the movement pattern of the natural organisms in a more realistic way. Meanwhile, self-sustained chaotic systems are of great significance for the optimization of nonlinear parametric systems, artificial neural networks [59], nonlinear time series and bionic robot, etc.

Currently, chaotic self-sustained systems base on active materials are seldom explored [55]. To realize more applications and functions, it is necessary to construct more self-sustained chaotic systems based on active materials, reveal their chaotic mechanism and behavior, and in turn provide guidance for the realization and control of self-sustained chaos. In fact, the construction of self-sustaining chaotic systems based on active materials is a very challenging task. Inspired by the classical Duffing chaotic system [58, 60], this paper constructs a self-floating system consisting of a nonlinear spring and a liquid crystal elastomer balloon, which is capable of self-beating under steady illumination due to self-shading effect [53,54]. Under steady illumination, the LCE balloon can float up and down in periodic or chaotic manner, where the joint action of buoyancy force and gravity on the balloon is similar to periodic external excitation in the Duffing equation [58,60]. This is a new kind of light-powered self-sustained chaotic system based on stimuli-responsive materials, being distinct from the previous periodic self-sustained oscillation system [47,54]. The objective of this paper is to construct a new type of chaotic self-sustained system using active material, reveal its self-sustained motion mechanism and chaotic mechanism, and provide guidance for the application of self-sustained chaotic motion of active materials in energy harvesters [20–23], self-cleaning [55], biomimetic robots [16,30], encrypted communication [60], etc.

This paper is written as follows. In Section 2, taking into account the well-established dynamic LCE model and ideal gas model, the corresponding governing equations of self-floating system and the beating dynamics of the LCE balloon are deduced. In Section 3, two motion regimes named static regime and self-floating regime are given by numerical calculation, and the mechanism of self-floating is explained. In Section 4, by adjusting the damping coefficient of the system, the evolution of the self-floating system from period to chaos is presented. Meanwhile, the time domain analysis and frequency domain analysis are carried out, and the Poincare map is drawn, with a more intuitive display of the chaotic evolution process. In Section 5, the influence of different system parameters on the self-floating is investigated in details. In Section 6, the conclusions are summarized.

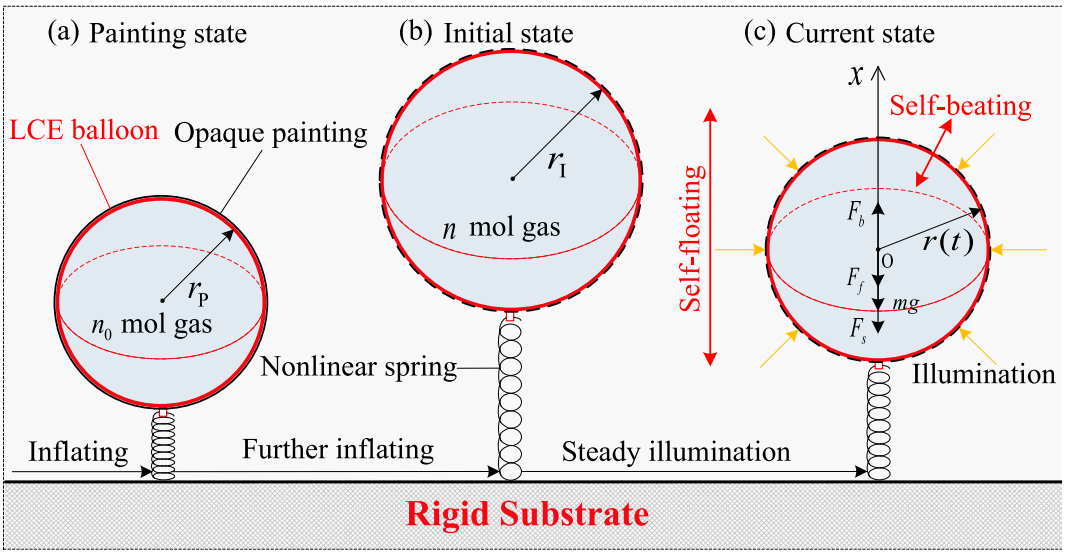

Fig. 1. Schematic of self-floating LCE balloon under steady illumination. (a) The original inflating state of the LCE balloon with painting radius r_P; (b) The initial state with radius r_I through further inflating and (c) The current state of the self-floating LCE balloon with arbitrary radius $r(t)$ under the steady illumination. The contraction and expansion of LCE balloon caused by the self-shading effect lead to the self-floating phenomenon.

2. Model and theoretical formulation

In this section, we first propose a light-powered chaotic self-floating system consisting of a nonlinear spring and a liquid crystal elastomer balloon, which is capable of self-beating under steady illumination due to self-shading effect. Then, the corresponding theoretical models are developed based on Newtonian dynamics and dynamic LCE model, in which it contains the governing equations of floating system, beating dynamics of the LCE balloon with shading coating, as well as the nondimensionalization of system parameters and solution method.

2.1. Governing equations of self-floating system

Fig. 1 sketches a self-floating system where a LCE balloon is attached to a nonlinear spring fixed on the rigid substrate and placed in steady illumination. In general, under light illumination LCE materials contract in the direction of the mesogen and expand in the other two directions. In Fig. 1, the balloon is made of a LCE membrane with in-plane isotropic patterning of director and a fine polydomain structure [61], so that the LCE balloon contracts in the plane and increases in the direction of thickness under illumination. Initially, the LCE balloon in stress-free state with the radius r_0 is inflated by n_0 mol ideal gas into the painting state with radius r_P and painted with an opaque power coating, as shown in Fig. 1(a). Then, the LCE balloon is further inflated to the initial state with radius r_I as shown in Fig. 1(b). In terms of the LCE material, the photochromic liquid crystal molecules can change from straight *trans* configuration to bent *cis* configuration caused by the light radiation or laser. Therefore, under illumination, the LCE balloon contracts with varying radius $r(t)$, as shown in Fig. 1(c). When $r(t) > r_P$, the LCE balloon contracts in response to illumination. When $r(t) \leq r_P$, the LCE balloon expands as the coating layer blocks the light. Finally, under steady illumination, the self-beating of the LCE balloon takes place, which is originated from the self-shading effect [53,54]. In the following, a theoretical model will be developed to study the behaviors of this self-floating system.

As illustrated in Fig. 1(c), the LCE balloon is subjected to the air buoyancy F_b, air damping force F_f, spring force F_s and gravity mg. The air buoyancy F_b is noted to always change with the radius of self-beating LCE balloon. In the Cartesian coordinate system, the governing equation for this self-floating system can be described by

$$m\ddot{x} = F_b - F_f - F_s - mg, \tag{1}$$

where m is the mass of the LCE balloon; $\ddot{x}$ refers to the acceleration of LCE balloon along the x axis and g is the acceleration of gravity. Hereon, to simplify the calculation, we assume a linear relationship between the air damping force and the velocity $\dot{x}$ of the LCE balloon with damping coefficient α as

$$F_f = \alpha\dot{x}. \tag{2}$$

For the sake of calculation, the center of the balloon when $F_b = mg$ is selected as the coordinate origin, as shown in Fig. 1(c). We further assume that the spring force of the nonlinear spring is

$$F_s = k\left(x - r(t) + \sqrt[3]{\frac{3m}{4\pi\rho_a}}\right)^3, \tag{3}$$

where k is the stiffness coefficient of the spring.

Considering that the thickness of the LCE balloon is much smaller than its radius, we suppose the buoyancy of the LCE balloon as

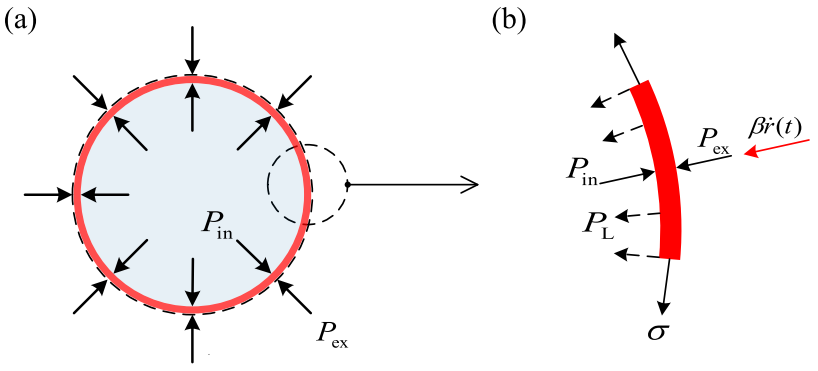

Fig. 2. Schematics of force analysis of LCE balloon. (a) The LCE balloon subjected to internal and external pressures and (b) The force analysis diagram of the micro element. The governing equation for periodic deformation of the LCE balloon can be determined under steady light illumination.

$$F_b = \frac{4\pi\rho_a g[r(t)]^3}{3}, \tag{4}$$

where ρ_a is the mass density of air.

Substituting Eqs. (2)–(4) into Eq. (1), we can obtain

$$m\ddot{x} = \frac{4\pi\rho_a g[r(t)]^3}{3} - \alpha\dot{x} - k\left(x - r(t) + \sqrt[3]{\frac{3m}{4\pi\rho_a}}\right)^3 - mg. \tag{5}$$

From Eq. (5), we can calculate the floating of LCE balloon, once the radius $r(t)$ of the beating LCE balloon is given. In the following, we further formulate the beating dynamics of the LCE balloon with shading coating.

2.2. Beating dynamics of the LCE balloon

Fig. 2 sketches the force analysis diagram of the balloon. Taking into account that the thickness of the LCE balloon is relatively thin, the effect of gravity on the LCE balloon deformation is ignored. Hereon, the spherical shell of LCE balloon is subjected to the internal gas pressure P_{in} and the external pressure P_{ex}, as shown in Fig. 2(a). To formulate the governing equation for the self-beating of LCE balloon, we take a micro element for the force analysis, in which there also exist the radial damping and Laplace pressure P_L from the membrane tension (caused by normal stress σ), as shown in Fig. 2(b). Therefore, we can obtain the governing equation for the self-beating of the LCE balloon as

$$\rho_L h\ddot{r}(t) = P_{in} - P_{ex} - P_L - \beta\dot{r}(t), \tag{6}$$

where $\ddot{r}$ and $\dot{r}$ represent the radial acceleration and velocity respectively; ρ_L and h denote the mass density and thickness of the LCE balloon respectively; β is the damping coefficient of radial deformation of the LCE balloon.

Assuming the gas in the LCE balloon to be an ideal gas, the internal pressure can be obtained by the Clapeyron equation

$$P_{in} = \frac{3nRT}{4\pi[r(t)]^3}, \tag{7}$$

where n, R and T are the amount of substance, gas constant and thermodynamic temperature of the ideal gas, respectively.

The Laplace pressure induced by membrane tension can be described as

$$P_L = \frac{2h\sigma(t)}{r(t)} = \frac{2hE\varepsilon(t)}{r(t)}, \tag{8}$$

where E and $\varepsilon(t)$ are elastic modulus of LCE balloon and elastic strain, respectively; h is the thickness of the LCE balloon. Hereon, for the sake of simplification the stress-strain relationship is assumed to be linear, although it is more complex in practice. And $h = V/4\pi r^2$ can be obtained through the assumption that LCE material is incompressible with its volume V being constant [54].

Substituting Eqs. (7) and (8) into Eq. (6), one can obtain

$$\rho_L h\ddot{r}(t) = \frac{3nRT}{4\pi[r(t)]^3} - P_{ex} - \frac{2hE\varepsilon(t)}{r(t)} - \beta\dot{r}(t), \tag{9}$$

in which

$$\varepsilon(t) = \frac{r(t) - r_0[1 + \varepsilon_L(t)]}{r_0[1 + \varepsilon_L(t)]}, \tag{10}$$

where $\varepsilon_L(t)$ is the effective light-driven strain of the LCE balloon.

The effective light-driven strain of the LCE balloon is assumed to be linearly as a function of the *cis* number fraction $\varphi(t)$ with contraction coefficient C, so we can obtain

$$\varepsilon_L(t) = -C\varphi(t). \tag{11}$$

Under the light-driven *trans*-to-*cis* excitation, the number fraction of bent *cis* isomers can be described as [62].

$$\frac{\partial\varphi(t)}{\partial t} = \eta_0 I_0(1 - \varphi(t)) - \frac{\varphi(t)}{T_0} \tag{12}$$

where I_0 and η_0 are the light intensity and light-absorption constant respectively; T_0 is the thermal relaxation time of LCE material from *cis* to *trans* state.

By solving Eq. (12) with considering the initial condition, the number fraction can be obtained as below

$$\varphi(t) = \frac{\eta_0 T_0 I_0}{\eta_0 T_0 I_0 + 1} + \left(\varphi_0 - \frac{\eta_0 T_0 I_0}{\eta_0 T_0 I_0 + 1}\right)\exp\left[-\frac{t}{T_0}(\eta_0 T_0 I_0 + 1)\right] \tag{13}$$

where φ_0 is the initial *cis* number fraction of photochromic molecules.

In this paper, the LCE balloon switches between an illumination state and a self-shading state. For Case I corresponding to the LCE balloon in the illumination state with initial $\varphi_0 = 0$, Eq. (13) can be simplified to

$$\varphi(t) = \frac{\eta_0 T_0 I_0}{\eta_0 T_0 I_0 + 1}\left\{1 - \exp\left[-(\eta_0 T_0 I_0 + 1)\frac{t_1}{T_0}\right]\right\}. \tag{14}$$

For Case II corresponding to the LCE balloon in the illumination state switched from self-shading state with transient $\varphi_0 = \varphi_{\text{shade}}$, Eq. (13) can be simplified to

$$\varphi(t) = \frac{\eta_0 T_0 I_0}{\eta_0 T_0 I_0 + 1} + \left(\varphi_{\text{shade}} - \frac{\eta_0 T_0 I_0}{\eta_0 T_0 I_0 + 1}\right)\exp\left[-(\eta_0 T_0 I_0 + 1)\frac{t_2}{T_0}\right]. \tag{15}$$

For Case III corresponding to the LCE balloon in the self-shading state ($I_0 = 0$) switched from illumination state with transient $\varphi_0 = \varphi_{\text{illum}}$, Eq. (13) can be simplified to

$$\varphi(t) = \varphi_{\text{illum}} \exp\left(-\frac{t_3}{T_0}\right), \tag{16}$$

where t_1, t_2 and t_3 are the durations of current process, respectively; φ_{shade} and φ_{illum} are the number fractions of *cis-isomers* at the switch moments from self-shading state into illumination state, and from illumination state into self-shading state, respectively.

2.3. Nondimensionalization

We introduce the following dimensionless parameters $\bar{\ddot{x}} = \frac{\ddot{x}}{g}$, $\bar{\dot{x}} = \frac{\dot{x}}{\sqrt{gr_0}}$, $\bar{x} = \frac{x}{r_0}$, $\bar{r} = \frac{r}{r_0}$, $\bar{r}_{\text{P}} = \frac{r_{\text{P}}}{r_0}$, $\bar{\rho}_{\text{a}} = \frac{4\pi\rho_{\text{a}} r_0^3}{3m}$, $\bar{k} = \frac{kr_0^3}{mg}$, $\bar{\alpha} = \frac{\alpha\sqrt{r_0}}{m\sqrt{g}}$, $\bar{t} = \frac{t}{T_0}$, $\bar{I}_0 = I_0\eta_0 T_0$, $\bar{n} = \frac{3nRT}{4\pi E r_0^3}$, $\bar{P}_{\text{ex}} = \frac{P_{\text{ex}}}{E}$, $\bar{\rho}_{\text{L}} = \frac{\rho_{\text{L}} r_0^2}{ET_0^2}$, $\bar{V} = \frac{V}{4\pi r_0^3}$ and $\bar{\beta} = \frac{\beta r_0}{ET_0}$, to rewrite the governing equation Eq. (5) as

$$\bar{\ddot{x}} = \bar{\rho}_{\text{a}}[\bar{r}(\bar{t})]^3 - \bar{\alpha}\bar{\dot{x}} - \bar{k}\left(\bar{x} - \bar{r}(\bar{t}) + \frac{1}{\bar{\rho}_{\text{a}}^{1/3}}\right)^3 - 1. \tag{17}$$

Substituting these dimensionless parameters into Eqs. 14–16, we can obtain the dimensionless equations of the *cis* number fraction,

For Case I,

$$\varphi(\bar{t}) = \frac{\bar{I}_0}{\bar{I}_0 + 1}\{1 - \exp[-(\bar{I}_0 + 1)\bar{t}_1]\}, \tag{18}$$

for Case II,

$$\varphi(\bar{t}) = \frac{\bar{I}_0}{\bar{I}_0 + 1} + \left(\varphi_{\text{shade}} - \frac{\bar{I}_0}{\bar{I}_0 + 1}\right)\exp[-(\bar{I}_0 + 1)\bar{t}_2], \tag{19}$$

and for Case III,

$$\varphi(\bar{t}) = \varphi_{\text{illum}} \exp(-\bar{t}_3), \tag{20}$$

It is noted that the LCE balloon is in self-shading state for $\bar{r} \le \bar{r}_{\text{P}}$, and in illumination state for $\bar{r} > \bar{r}_{\text{P}}$.

Substituting Eqs. (10) and (11) into Eq. (9), we can get

Table 1
Material properties and geometric parameters.

Parameter	Definition	Value	Units
r_0	Initial radius	1–30	m
ρ_{a}	Mass density of air	1.29	kg/m^3
ρ_{L}	Mass density of LCE	900–1300	kg/m^3
α	System damping coefficient	2000–20,000	kg/s
β	Deformation damping coefficient	2000–8000	s · Pa/m
k	Stiffness coefficient of the spring	1.5–15	kg/m^2 · s^2
I_0	Light intensity	10–40	kW/m^2
C	Contraction coefficient	0.1–0.5	/
T_0	Thermal relaxation time	0.1–0.2	s
η_0	Light-absorption constant	0.00022	m^2/s · W
E	Young's modulus	1–10	MPa
P_{ex}	External pressure	0.1–1.35	MPa

$$\ddot{\bar{r}}(\bar{t}) = \frac{\bar{n}}{[\bar{r}(\bar{t})]\bar{\rho}_L \bar{V}} - \frac{\bar{p}_{ex}[\bar{r}(\bar{t})]^2}{\bar{\rho}_L \bar{V}} - 2\frac{\dot{\bar{r}}(\bar{t}) - 1 + C\varphi(\bar{t})}{\bar{r}(\bar{t})\bar{\rho}_L(1 - C\varphi(\bar{t}))} - \frac{\bar{\beta}[\bar{r}(t)]^2}{\bar{\rho}_L \bar{V}}\dot{\bar{r}}(\bar{t}). \tag{21}$$

From Eqs. 18–21, the radius of the LCE balloon in three cases can be obtained. It should be mentioned here that it is difficult to find analytical solutions to the governing equations (17) and (21) with variable coefficient. Hereon, the four-order Runge-Kutta method is adopted to solve the above differential equations with the help of Matlab software. Based on the existing experiments [63], Table 1 and Table 2 gather the typical values of the required parameters in current paper and the corresponding dimensionless parameters, respectively.

3. Periodic self-floating and its mechanism

In this section, based on the afore established theoretical models, we further present two typical motion regimes of the light-powered floating balloon, i.e., the static regime and self-floating regime. The motion regime of the LCE balloon depends to a great extent on the system parameters. Hereon, we will study the floating behaviors of LCE balloon with different painting radii and reveal the corresponding motion mechanism.

3.1. Periodic self-floating

To study the dynamic behaviors of self-floating system under steady illumination, the time-history and phase diagrams for distinct $\bar{r}_P$ are portrayed in Fig. 3, in which the other system dimensionless parameters are selected as follows: $\bar{\rho}_a = 0.65$, $\bar{\rho}_L = 2.5$, $\bar{k} = 0.05$, $\bar{\alpha} = 0.2$, $\bar{\beta} = 0.1$, $\bar{I}_0 = 0.2$, $C = 0.2$, $\bar{n} = 0.5$, $\bar{V} = 0.8$ and $\bar{P}_{ex} = 0.1$. Through numerical calculations, two typical motion regimes, i.e., static regime and self-floating regime, are found as shown in Fig. 3. For the painting radius $\bar{r}_P = 1$, the floating balloon ends up in static regime. The corresponding time-history and phase trajectory are plotted in Fig. 3(a) and (b), respectively. The floating system finally comes to rest due to the damping energy dissipation. Whereas, for the painting radius $\bar{r}_P = 1.2$, the floating balloon ends up in self-floating regime, with the corresponding time-history and phase trajectory displaying in Fig. 3(c) and (d), respectively. The velocity point in the phase plane will eventually appear as a limit cycle as shown in Fig. 3(d). This result means that the balloon can self-float up and down continuously and periodically under steady illumination. We attribute this to the fact that the damping energy dissipation is compensated by the work done by buoyancy of the LCE balloon. The mechanism of this phenomenon will be explained in details by calculating several key quantities of the system during self-floating in Section 3.2.

3.2. Mechanism of self-floating

To reveal the self-floating mechanism of LCE balloon system, Fig. 4 plots the relations among the number fraction, radius, buoyancy and displacement of the LCE balloon with the dimensionless parameters: $\bar{r}_P = 1.2$; $\bar{\rho}_a = 0.65$, $\bar{\rho}_L = 2.5$, $\bar{k} = 0.05$, $\bar{\alpha} = 0.2$, $\bar{\beta} = 0.1$, $\bar{I}_0 = 0.2$, $C = 0.2$, $\bar{n} = 0.5$, $\bar{V} = 0.8$ and $\bar{P}_{ex} = 0.1$, in which the yellow shaded area denotes the LCE balloon in the illumination state, i.e., $\bar{r} > \bar{r}_P = 1.2$. Fig. 4(a) plots the time dependence of the *cis* number fraction $\bar{\varphi}$ in the LCE balloon. The *cis* number fraction $\bar{\varphi}$ is observed to vary periodically between the illumination state and self-shading state. This periodic change of number fraction results in a periodic change in the balloon radius as shown in Fig. 4(b). Meanwhile, the change of the radius leads to the change in its volume, which in turn causes the periodic change in buoyancy as shown in Fig. 4(c). In the process of self-floating, sufficient external energy must be supplied to the system to offset the energy dissipated by damping to maintain the self-sustained motion of the system. Fig. 4(d) shows the displacement dependence of the buoyancy of LCE balloon, in which the red grid area surrounded by a closed loop represents the work done by the buoyancy of LCE balloon. Actually, this net energy arises from the periodic expansion/contraction of the beating LCE balloon under steady illumination. Based on this self-shading-expansion mechanism [53,54], the LCE balloon will present a continuous self-sustained floating, as long as the net energy input to the system with proper parameters can compensate for the energy dissipated by the damping.

4. Evolution of chaotic self-floating

In the previous section, the LCE balloon system can maintain a periodic and continuous floating under steady illumination. Actually, the balloon system is also able to undergo a chaotic self-sustained floating under steady illumination. In this section, we will further illustrate the evolution process of self-sustained chaotic floating through single-period, double-period and multi-period self-floating, by the continuous adjustment of the damping coefficient $\bar{\alpha}$ in details.

Table 2
Dimensionless parameters.

Parameter	$\bar{\rho}_a$	$\bar{\rho}_L$	$\bar{\alpha}$	$\bar{\beta}$	$\bar{k}$	$\bar{I}_0$	$\bar{n}$	$\bar{V}$	$\bar{P}_{ex}$
Value	0.1–0.8	1–10	0–0.2	0–0.2	0.02–0.2	0–0.5	0.4–0.6	0.02–1	0–0.15

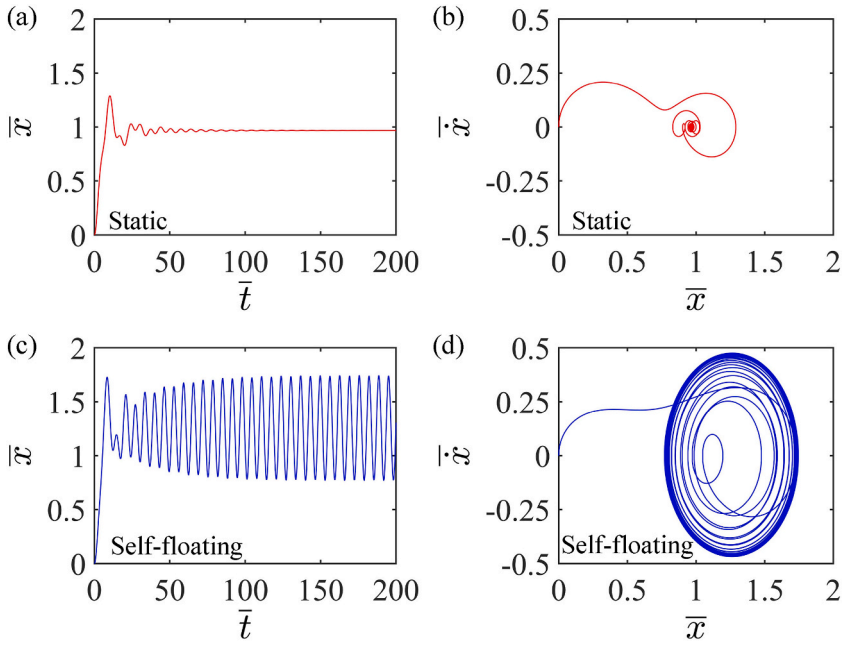

Fig. 3. Two typical regimes: static regime and self-floating regime. (a) Time-history of the displacement with $\bar{r}_P = 1.0$; (b) Phase diagram with $\bar{r}_P = 1.0$; (c) Time-history of the displacement with $\bar{r}_P = 1.2$ and (d) Phase diagram with $\bar{r}_P = 1.2$.

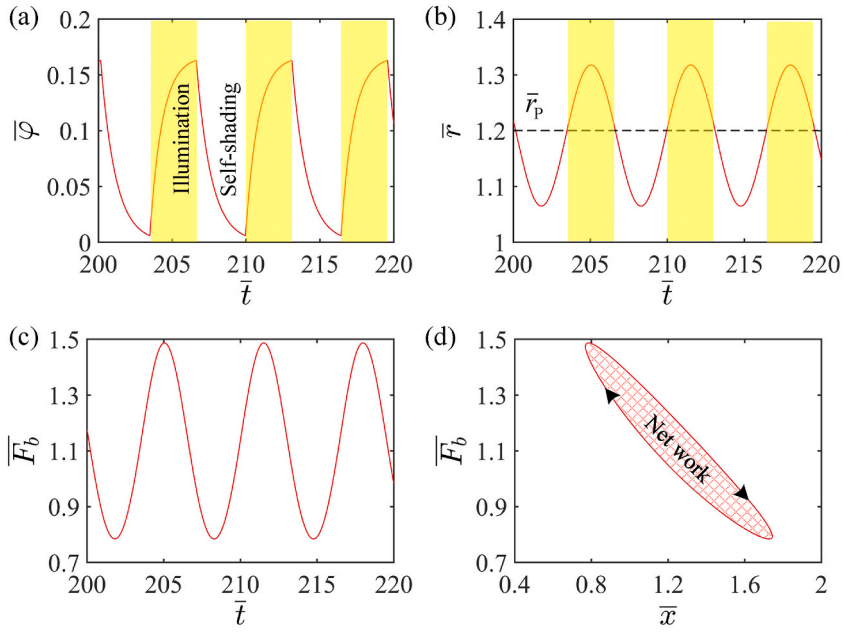

Fig. 4. Explanatory mechanism diagrams of self-floating of LCE balloon. (a) Time dependence of the number fraction; (b) Time dependence of the balloon radius; (c) Time dependence of the buoyancy of the balloon and (d) Displacement dependence of the buoyancy of the balloon. The self-floating mechanism can be summarized simply as the work done by buoyancy compensating the damping energy dissipation.

4.1. Single-period self-floating

Fig. 5 portrays the time-history curve, limit cycle, frequency spectrum and Poincare map of the single-period self-floating of the LCE balloon for damping coefficient $\bar{\alpha} = 0.2$, in which the other dimensionless parameters are selected as follows: $\bar{\rho}_a = 0.65, \bar{\rho}_L = 2.5, \bar{k} = 0.05, \bar{\beta} = 0.1, \bar{I}_0 = 0.2, C = 0.2, \bar{n} = 0.5, \bar{V} = 0.8$ and $\bar{P}_{ex} = 0.1$. With the observation of Fig. 5(a), the LCE balloon develops into self-floating with constant amplitude and frequency. This is a simple case where the LCE balloon floats with a single period. Fig. 5(b) plots

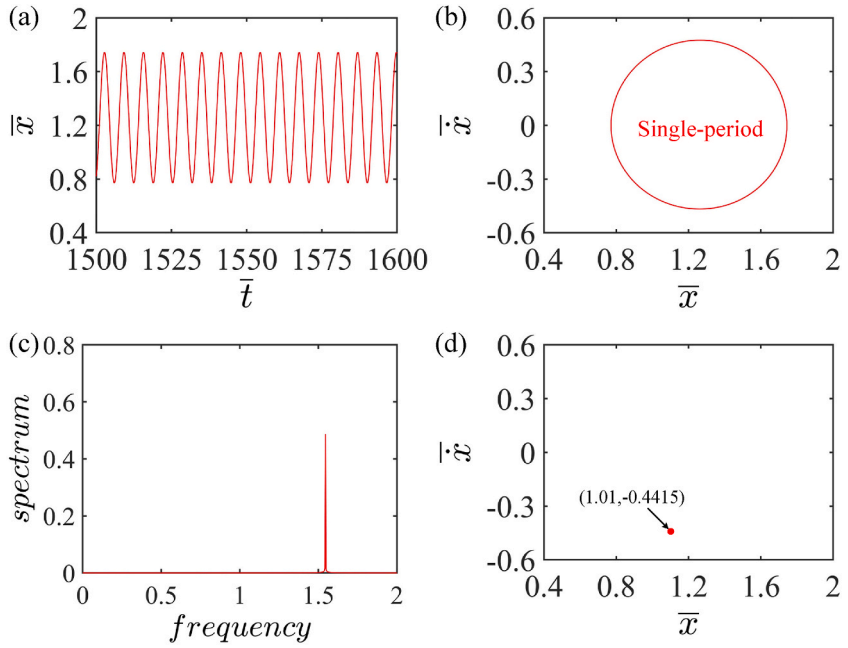

Fig. 5. Single-period self-floating regime of LCE balloon. (a) Time-history curve; (b) Limit cycle in the phase diagram; (c) Frequency spectrum and (d) Poincare map. Results show that the self-sustained floating of LCE balloon is single-period under the present dimensionless parameters.

the corresponding limit cycle of this single-period self-floating. As can be seen, there is only one limit cycle in the steady self-floating state. This also means that the self-floating of LCE balloon is a single period. Hereon, the frequency spectra and Poincare map are further depicted for the behavior study of self-floating. Fig. 5(c) plots the frequency spectrum of the self-floating of the LCE balloon. There is one sharp power spectra, indicating that the LCE balloon floats periodically. Fig. 5(d) plots the Poincare map of self-floating, in which the plane with $\bar{r} = 1.2$ is chosen as the Poincare section. A fixed point (1.01, −0.4415) on the Poincare section at this time, further confirms that this is a single-period floating. Generally, for a single-period floating regime of the LCE balloon, the floating period can be easily identified by using time-history curve or phase diagram, but for complex floating states, it is necessary to judge the

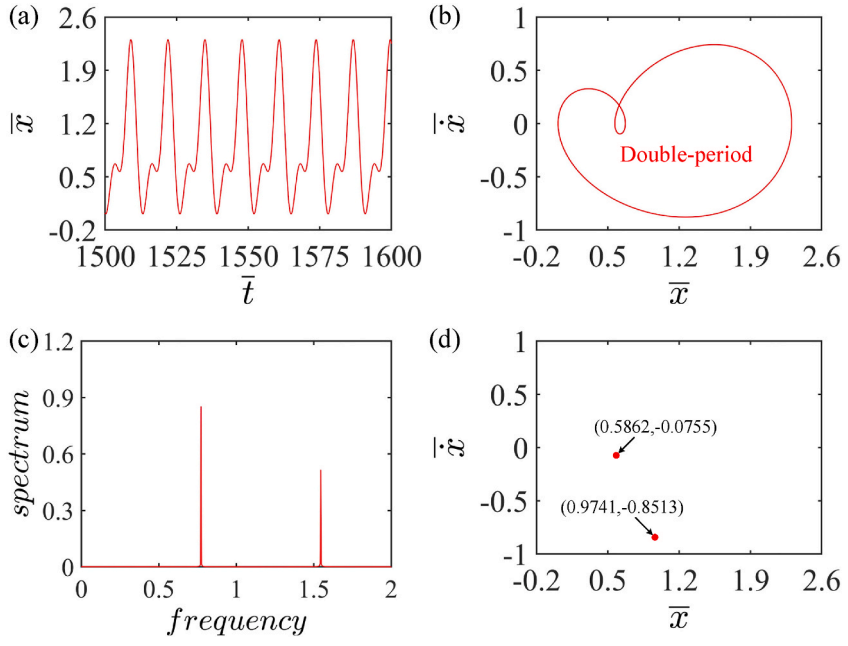

Fig. 6. Double-period self-floating regime of LCE balloon. (a) Time-history curve; (b) Limit cycle in the phase diagram; (c) Frequency spectrum and (d) Poincare map. Results show that the self-floating of LCE balloon is double-period under the present dimensionless parameters.

floating behaviors, such as chaos, with the help of frequency spectrum or Poincare map.

4.2. Double-period self-floating

With the further research, new self-sustained floating phenomena are found by reducing the damping coefficient. Hereon, the time-history curve, limit cycle, frequency spectrum and Poincare map of the self-floating of LCE balloon for $\overline{\alpha} = 0.1$ are portrayed in Fig. 6, in which the other dimensionless parameters are selected as follows: $\overline{\rho}_a = 0.65$, $\overline{\rho}_L = 2.5$, $\overline{k} = 0.05$, $\overline{\beta} = 0.1$, $\overline{I}_0 = 0.2$, $C = 0.2$, $\overline{n} = 0.5$, $\overline{V} = 0.8$ and $\overline{P}_{ex} = 0.1$. Fig. 6(a) plots the time-history curve of the self-sustained floating, in which we look closely to find that the LCE balloon floats with two different amplitudes. This means that the LCE balloon is self-floating with a double period. Fig. 6(b) plots the limit cycle of the self-sustained floating. Clearly seen that the limit cycle is a closed two-turn coil, also indicating that the self-sustained floating of LCE balloon is double-period. Hereon, the frequency spectra and Poincare map are also plotted to investigate the behaviors of self-sustained floating. Fig. 6(c) plots the frequency spectrum of self-sustained floating of the LCE balloon. Although a secondary frequency is generated in addition to the primary frequency, they are sharp and separated, suggesting that the self-sustained floating of the LCE balloon is still periodic. Fig. 6(d) plots the Poincare map of self-sustained floating, in which the plane with $\overline{r} = 1.2$ is chosen as the Poincare section. There exist two fixed points (0.5862, −0.0755) and (0.9741, −0.8513) on the Poincare section at this time, which further confirms the double-period floating. For the double-period floating regime of the LCE balloon, to judge the floating period by using phase diagram or Poincare map is a better approach than the time history or frequency spectrum.

Similar to the single-period self-floating (Fig. 4(d)), Fig. 7 shows the displacement dependences of the buoyancy of LCE balloon for the double-period self-floating and four-period self-floating, in which the red grid area and blue grid area represent the positive work and negative work respectively, and the numbers of 1 to 4 or 1 to 8 represent the cyclic path of buoyancy. It is seen that the work done by the double-period self-floating differs from that done by the single-period by comparing Figs. 7(a) and Fig. 4(d). The law of work done by four-period self-floating is similar to that of work done by double-period self-floating as shown in Fig. 7(b). For the double-period or four-period self-floating, the net work resulting from the superposition of positive and negative work is inputted to the system to compensate the damping dissipation and maintain the self-floating under steady illumination. For the following multi-period or chaotic self-floating, the energy compensation mechanism is similar to that of the double-period or four-period self-floating.

4.3. Multi-period self-floating

Through further reduction of the damping coefficient, the self-sustained floating of LCE balloon is found to appear a multi-period situation. Similarly, the time-history curve, limit cycle, frequency spectrum and Poincare map of the self-floating of the LCE balloon for $\overline{\alpha} = 0.028$ are portrayed in Fig. 8, in which the other dimensionless parameters are selected as follows: $\overline{\rho}_a = 0.65$, $\overline{\rho}_L = 2.5$, $\overline{k} = 0.05$, $\overline{\beta} = 0.1$, $\overline{I}_0 = 0.2$, $C = 0.2$, $\overline{n} = 0.5$, $\overline{V} = 0.8$ and $\overline{P}_{ex} = 0.1$. Fig. 8(a) plots the time-history curve of self-sustained floating, in which the amplitude changes slightly with a certain regularity. In this case, the LCE balloon shows a multi-period floating. Fig. 8(b) plots the corresponding limit cycle of self-sustained floating. The limit cycle is observed to change into a closed multi-turn coil, referring to the multi-period self-floating. Hereon, the frequency spectra and Poincare map are further plotted to study the behaviors of self-floating. Fig. 8(c) plots the frequency spectrum of self-sustained floating of the LCE balloon. With the increase of the period, except for the primary frequency, the floating frequency of the balloon alters continuously in the lower amplitude region, which indicates that the self-floating of the LCE balloon at current time will be the beginning of chaos [58]. Fig. 8(d) plots the corresponding Poincare map of self-floating, in which the plane with $\overline{r} = 1.2$ is chosen as the Poincare section. There is a small area on the section of Poincare at this time, suggesting that the number of floating periods is increasing, and the self-floating of the balloon gradually evolves towards chaos. This further confirms that the self-sustained floating is the multi-period floating.

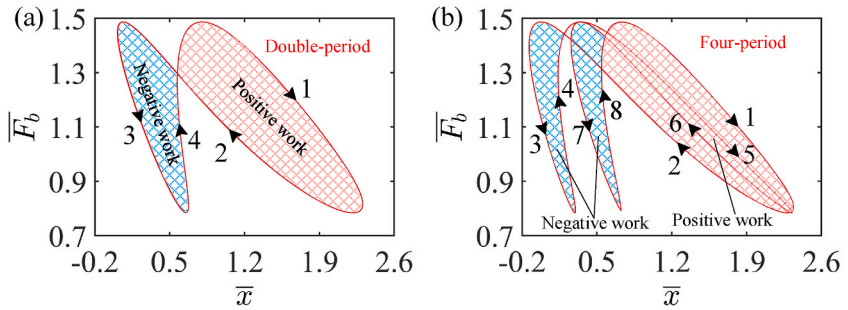

Fig. 7. The displacement dependences of the buoyancy of LCE balloon for (a) double-period self-floating and (b) four-period self-floating. The net work resulting from the superposition of positive and negative work is inputted to the system to compensate the damping dissipation and maintain the self-floating under steady illumination.

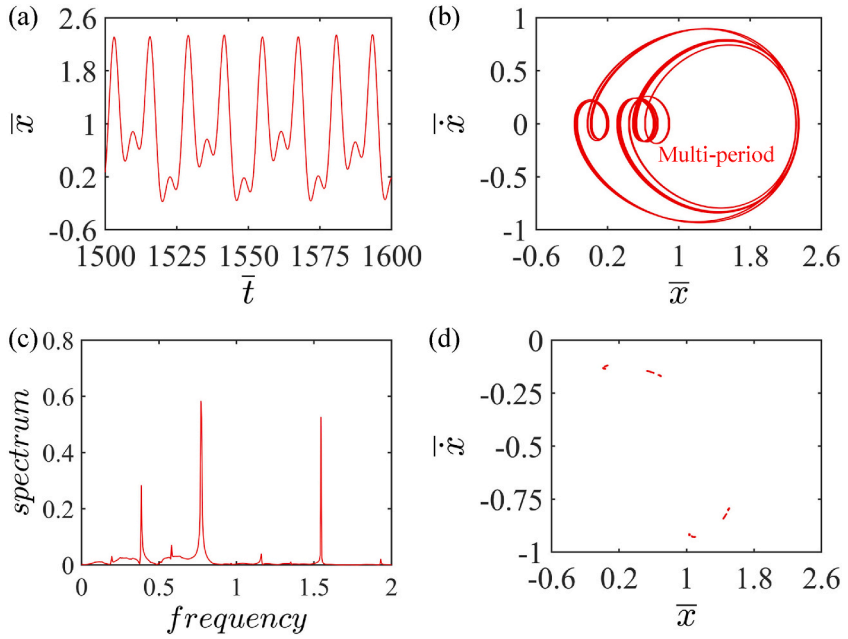

Fig. 8. Multi-period self-floating regime of LCE balloon. (a) Time-history curve; (b) Limit cycle in the phase diagram; (c) Frequency spectrum and (d) Poincare map. Results show that the self-floating of LCE balloon is multi-period under the present dimensionless parameters.

4.4. Chaotic self-floating

By further reducing the damping coefficient, we find that the self-floating of LCE balloon exhibits chaotic phenomenon. We still portray the time-history curve, attractor, frequency spectrum and Poincare map of the self-floating of the LCE balloon for $\overline{\alpha} = 0.02$ in Fig. 9, where the other dimensionless parameters are selected as follows: $\overline{\rho}_{\mathrm{a}} = 0.65$, $\overline{\rho}_{\mathrm{L}} = 2.5$, $\overline{k} = 0.05$, $\overline{\beta} = 0.1$, $\overline{I}_0 = 0.2$, $C = 0.2$, $\overline{n} = 0.5$, $\overline{V} = 0.8$ and $\overline{P}_{\mathrm{ex}} = 0.1$. Fig. 9(a) plots the time-history curve of self-sustained floating, in which the curve becomes complicated and irregular. In this case, the floating of LCE balloon is obviously chaotic. Fig. 9(b) plots the attractor of self-sustained

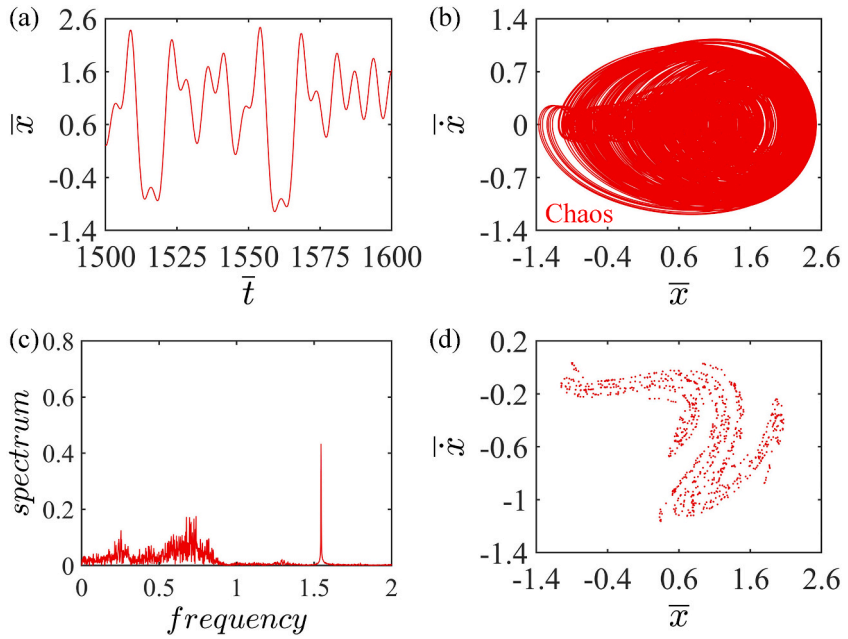

Fig. 9. Chaotic phenomena of LCE balloon. (a) Time-history curve; (b) Attractor in the phase diagram; (c) Frequency spectrum and (d) Poincare map. Results show that the self-floating of LCE balloon is the chaotic floating under the present dimensionless parameters.

floating. The attractor becomes complex, and the floating no longer has a periodic trajectory, indicating that the floating of the balloon at this time is chaotic. The fractal structure appears on the attractor, which is an important characteristic of chaos [64]. Hereon, the frequency spectra and Poincare map are further portrayed for the behavior research of self-sustained floating. Fig. 9(c) plots the frequency spectrum of self-sustained floating of the LCE balloon. More peaks and continuous frequencies appear in the frequency spectrum, reflecting the aperiodic nature of the chaos phenomenon. Fig. 9(d) plots the Poincare map of self-sustained floating, in which the plane with $\bar{r} = 1.2$ is chosen as the Poincare section. The Poincare section has a more complex pattern, and a distinct attraction domain emerges. This further confirms that the self-sustained floating is the chaotic floating.

It should be mentioned here that one-dimensional bifurcation diagram is further plotted to explore the dynamic evolution of the chaotic phenomenon of self-floating with continuously changing damping coefficients, as shown in Fig. 10. For $\bar{\alpha} > 0.184$, the self-floating of LCE balloon is a single-period motion. For $0.064 < \bar{\alpha} < 0.184$, the self-floating of LCE balloon is a double-period motion. For $0.033 < \bar{\alpha} < 0.064$, the self-floating of LCE balloon is a four-period motion. For $\bar{\alpha} < 0.033$, the self-floating of LCE balloon is a chaotic system. This system is observed to be typically period-doubling bifurcated into chaos. The chaotic phenomenon found in current study is investigated based on different damping parameters, and the effect of other parameters on the floating regime of the LCE balloon will be discussed in Section 5.

5. Effect of system parameters on self-floating

To focus on the study of chaotic phenomena, this section only discusses the self-sustained floating regime, and the selected parameters have certain pertinence, that is, all the selected parameters can make the system reach the self-sustained floating regime. Meanwhile, due to the emergence of multi-period and chaotic phenomena, the floating amplitude of time-history curve is not unique. Therefore, in order to better describe the floating behavior, we introduce the concept of average amplitude [65]. In the following, we will discuss the influence of each parameter on chaos one by one.

5.1. *Effect of the air mass density*

This section mainly discusses the effect of air mass density on chaotic phenomena of self-sustained floating. Hereon, the time-history curve, phase diagram and Poincare map for different $\bar{\rho}_a$ are portrayed in Fig. 11, in which the other dimensionless parameters are selected as follows: $\bar{\rho}_L = 2.5$, $\bar{k} = 0.05$, $\bar{\alpha} = 0.02$, $\bar{\beta} = 0.1$, $\bar{I}_0 = 0.2$, $C = 0.3$, $\bar{n} = 0.5$, $\bar{V} = 0.6$ and $\bar{P}_{ex} = 0.1$. The value of air mass density is found to affect the appearance of chaotic phenomenon. By comparing Fig. 11(a), (d) and (g), it can be found that with the increase of air mass density $\bar{\rho}_a$, the time-history curve changes from order to disorder, and then to order again, in addition, the floating amplitude becomes smaller with positions moving up due to the increased buoyancy. By comparing Fig. 11(b), (e) and (h), it can be also found that with the increase of $\bar{\rho}_a$, the phase diagram varies from simple to complex, and then to simple again. These results demonstrate that neither too small nor too large air mass density will cause chaotic phenomenon. In the comparison of Fig. 11(c), (f) and (i), with the increase of $\bar{\rho}_a$, the points on the Poincare diagram evolve from single to multiple, and then back to single. The Poincare map in Fig. 11(f) shows that chaotic phenomenon of the self-sustained floating system appears with the dimensionless parameter $\bar{\rho}_a = 0.6$. Further calculations reveal that chaotic phenomenon will occur when the dimensionless density parameter is in the interval of 0.599–0.605. This may be attributable to the fact that too small air density is unable to generate enough driving force caused by buoyancy to promote the system to produce chaotic phenomena, and finally the LCE balloon will self-float near the low potential well (Fig. 11(a)). Conversely, if the air density is too large, the buoyancy of the system will be much larger than the damping force, so that the motion of the entire system is limited by the buoyancy, and finally the LCE balloon will self-float near the high potential well (Fig. 11(g)).

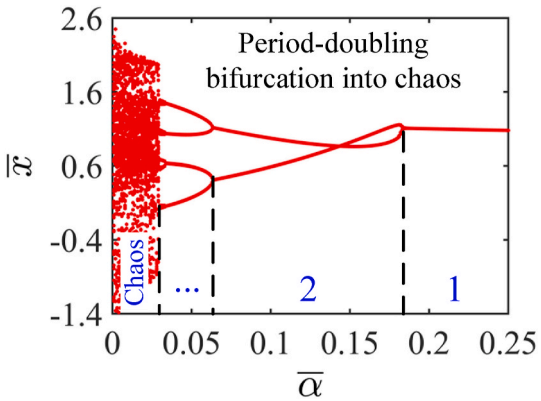

Fig. 10. One-dimensional bifurcation diagram of the self-floating system. The chaos of the self-floating comes from period-doubling bifurcation.

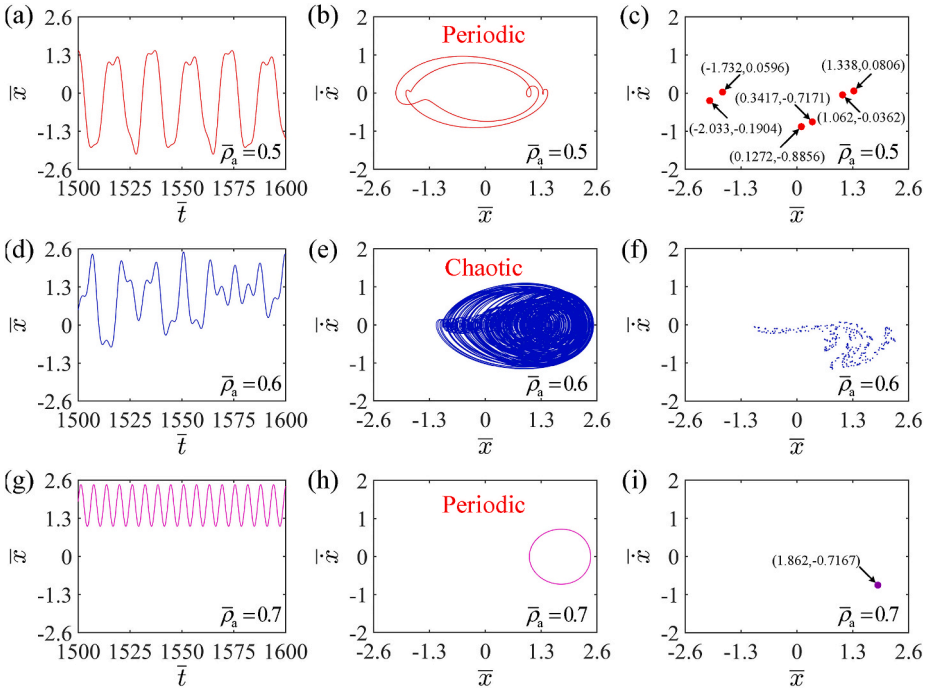

Fig. 11. Self-sustained floating behaviors of LCE balloon with different dimensionless air densities. (a) Time-history curve, (b) Limit cycle in the phase diagram, and (c) Poincare map with $\bar{\rho}_a = 0.5$;(d) Time-history curve, (e) Attractor in the phase diagram, and (f) Poincare map with $\bar{\rho}_a = 0.6$; (g) Time-history curve, (h) Limit cycle in the phase diagram, and (i) Poincare map with $\bar{\rho}_a = 0.7$.

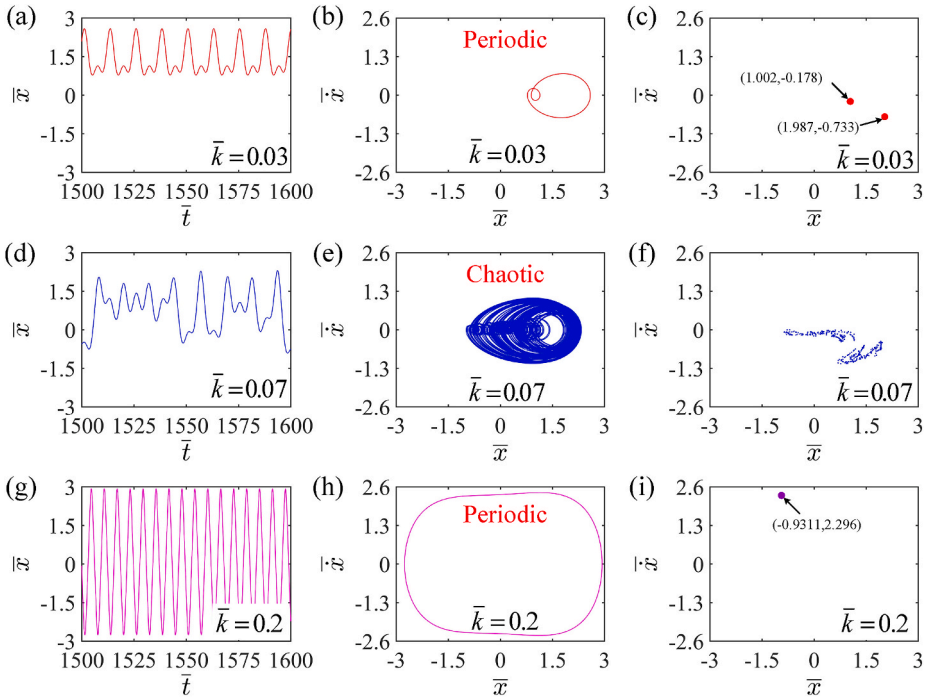

Fig. 12. Self-sustained floating behaviors of LCE balloon with different dimensionless spring stiffness coefficients. (a) Time-history curve, (b) Limit cycle in the phase diagram, and (c) Poincare map with $\bar{k} = 0.03$;(d) Time-history curve, (e) Attractor in the phase diagram, and (f) Poincare map with $\bar{k} = 0.07$;(g) Time-history curve, (h) Limit cycle in the phase diagram, and (i) Poincare map with $\bar{k} = 0.2$.

5.2. Effect of the spring stiffness coefficient

This section mainly studies the spring stiffness coefficient affecting chaotic phenomena of self-sustained floating. Hereon, Fig. 12 displays the time-history curve, phase diagram and Poincare map for different $\bar{k}$, where the other dimensionless parameters are selected as follows: $\bar{\rho}_a = 0.6$, $\bar{\rho}_L = 2.5$, $\bar{\alpha} = 0.02$, $\bar{\beta} = 0.1$, $\bar{I}_0 = 0.2$, $C = 0.3$, $\bar{n} = 0.5$, $\bar{V} = 0.6$ and $\bar{P}_{ex} = 0.1$. Easily observed that the value of stiffness coefficient has an impact on the occurrence of chaotic phenomenon. The comparison among Fig. 12(a), (d) and (g) turns out that with the increase of stiffness coefficient, the time-history curve changes from order to disorder, and then to order again, furthermore, the floating amplitude of the LCE balloon becomes larger and larger, and the floating positions move down due to the increase of spring restoring force. By comparing Fig. 12(b), (e) and (h), the phase diagram is found to change from simple to complex, and then to simple again with the increase of stiffness coefficient. Concluded from the comparison of Fig. 12(c), (f) and (i), the points on the Poincare diagram change from single to multiple, and then to single with the increase of stiffness coefficient. The Poincare map in Fig. 12(f) shows that chaotic phenomenon of the self-sustained floating system occurs at $\bar{k} = 0.07$. Through the numerical calculations, it is found that when the dimensionless stiffness coefficient parameter is in the range of 0.05–0.17, chaotic phenomenon of the self-sustained floating will appear. For too small or too large stiffness coefficient of the spring, the system will not exhibit chaotic phenomenon. The reason is that the generation of chaos requires switching between high and low potential wells. For too small or too large stiffness coefficient, buoyancy or spring force plays a dominant role, thus chaotic phenomenon will not occur.

5.3. Effect of the light intensity

This section presents a mainly discussion on the effect of light intensity on chaotic phenomena of self-sustained floating. Hereon, the time-history curve, phase diagram and Poincare map for different $\bar{I}_0$ are portrayed in Fig. 13, in which the other dimensionless parameters are selected as follows: $\bar{\rho}_a = 0.6$, $\bar{\rho}_L = 2.5$, $\bar{k} = 0.05$, $\bar{\alpha} = 0.02$, $\bar{\beta} = 0.05$, $C = 0.2$, $\bar{n} = 0.5$, $\bar{V} = 0.7$ and $\bar{P}_{ex} = 0.1$. It can be found from Fig. 13 that the appearance of chaotic phenomenon is affected by the value of light intensity. By comparing Fig. 13(a), (d) and (g), the time-history curve undergoes a change from order to disorder, and then to order again with the increase of light intensity. Furthermore, the floating amplitude is increased since the increase of the light intensity promotes the change of buoyancy. Similarly, by comparing Fig. 13(b), (e) and (h), the phase diagram displays a variation from simple to complex, and then to simple again with the increase of light intensity. Combined Fig. 13(c), (f) and (i), the number of points on the Poincare diagram alters from single to multiple, and then to single with the increase of light intensity. The Poincare map in Fig. 13(f) reveals that chaotic phenomenon of the self-sustained floating system appears at $\bar{I}_0 = 0.17$. It is concluded by numerical calculations that when the light intensity is in the range of 0.12–0.22, chaotic phenomenon of the self-sustained floating will take place. The results demonstrate that neither too small

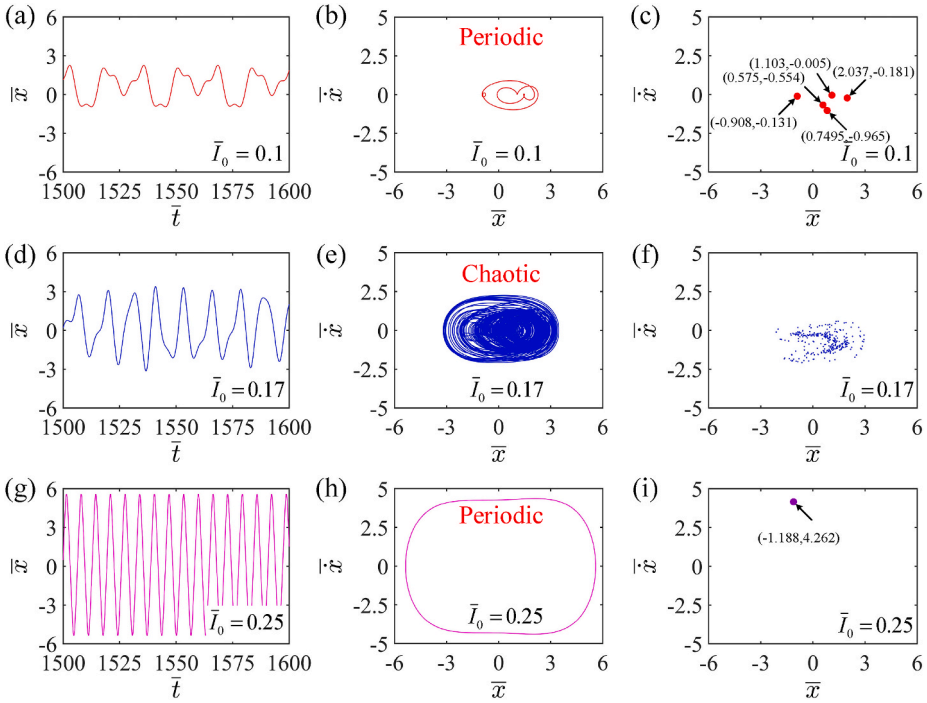

Fig. 13. Self-sustained floating behaviors of LCE balloon with different dimensionless light intensities. (a) Time-history curve, (b) Limit cycle in the phase diagram, and (c) Poincare map with $\bar{I}_0 = 0.1$; (d) Time-history curve, (e) Attractor in the phase diagram, and (f) Poincare map with $\bar{I}_0 = 0.17$; (g) Time-history curve, (h) Limit cycle in the phase diagram, and (i) Poincare map with $\bar{I}_0 = 0.25$.

nor too large light intensity will result in chaotic phenomenon. This phenomenon can be understood by analogy with the influence of spring modulus. For too small or too large light intensity, spring force or buoyancy is dominant, thus chaotic phenomenon will not take place.

5.4. Effect of the contraction coefficient

This section mainly discusses the effect of contraction coefficient on chaotic phenomena of self-sustained floating. Hereon, the time-history curve, phase diagram and Poincare map for different C are presented in Fig. 14, where the other dimensionless parameters are selected as follows: $\overline{\rho}_{\mathrm{a}} = 0.6$, $\overline{\rho}_{\mathrm{L}} = 2.5$, $\overline{k} = 0.05$, $\overline{\alpha} = 0.02$, $\overline{\beta} = 0.07$, $\overline{I}_0 = 0.2$, $\overline{n} = 0.5$, $\overline{V} = 0.7$ and $\overline{P}_{\mathrm{ex}} = 0.1$. Fig. 14 indicates that the value of contraction coefficient affects the appearance of chaotic phenomenon. Summarized from the comparison among Fig. 14 (a), (d) and (g), the time-history curve experiences a change from order to disorder, and then to order again along with the increased contraction coefficient. Moreover, the floating amplitude is getting larger since the change of buoyancy is promoted owing to the increase of the contraction coefficient. Similarly, the comparison among Fig. 14(b), (e) and (h) turns out that the phase diagram varies from simple to complex, and then to simple again with the increase of contraction coefficient. For Fig. 14(c), (f) and (i), the points on the Poincare diagram exhibit a number variation from single to multiple, and then to single with the increase of contraction coefficient. The Poincare map in Fig. 14(f) shows that chaotic phenomenon of the self-exited floating system occurs at $C = 0.25$. Numerical calculations lead to the conclusion that when the contraction coefficient is between 0.18 and 0.31, chaotic phenomenon of the self-sustained floating will emerge. For too small or too large contraction coefficient, the system will not appear chaotic phenomenon. This is similarly attributed to the fact that for too small or too large contraction coefficient, spring force or buoyancy plays a cardinal role, thus the LCE balloon finally self-floats near the low or high potential wells.

5.5. Effect of the external pressure

In this section, the effect of external pressure on chaotic phenomena of self-sustained floating is investigated. Hereon, Fig. 15 presents the time-history curve, phase diagram and Poincare map for different $\overline{P}_{\mathrm{ex}}$, in which the other dimensionless parameters are selected as follows: $\overline{\rho}_{\mathrm{a}} = 0.6$, $\overline{\rho}_{\mathrm{L}} = 2.5$, $\overline{k} = 0.05$, $\overline{\alpha} = 0.02$, $\overline{\beta} = 0.1$, $\overline{I}_0 = 0.2$, $C = 0.3$, $\overline{n} = 0.5$ and $\overline{V} = 0.6$. The value of external pressure is observed to have an influence on the occurrence of chaotic phenomenon. Observed from the comparison among Fig. 15(a), (d) and (g), the time-history curve alters from order to disorder, and then to order again with the increasing external pressure. In addition, the floating amplitude becomes decreased since the increase of external pressure restrains the change of buoyancy. By comparing Fig. 15(b), (e) and (h), it can be also found that the phase diagram changes from simple to complex, and then to simple again

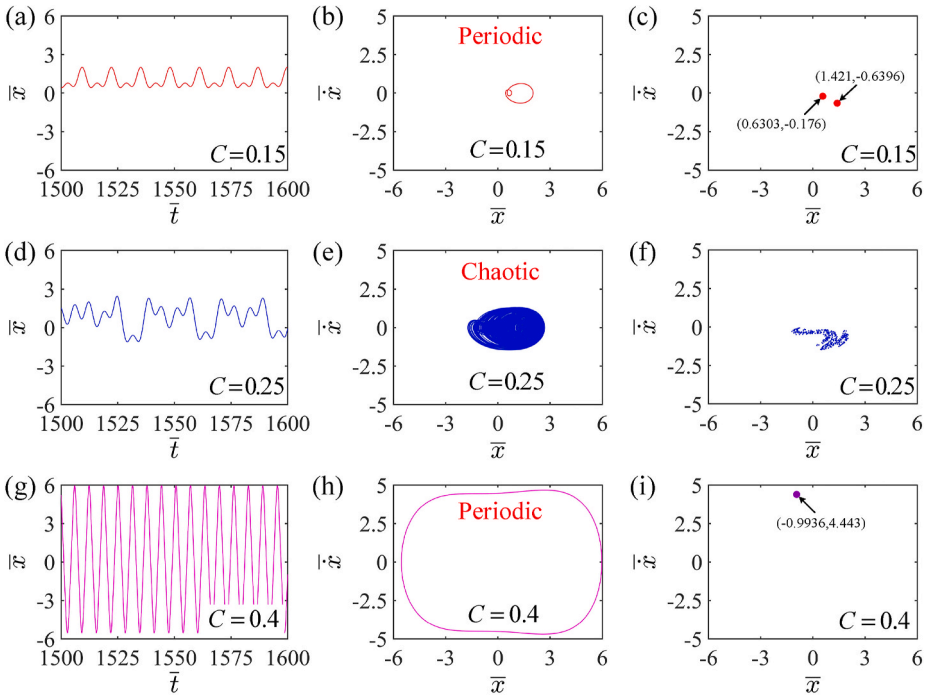

Fig. 14. Self-sustained floating behaviors of LCE balloon with different dimensionless contraction coefficients. (a) Time-history curve, (b) Limit cycle in the phase diagram, and (c) Poincare map with $C = 0.15$;(d) Time-history curve, (e) Attractor in the phase diagram, and (f) Poincare map with $C = 0.25$;(g) Time-history curve, (h) Limit cycle in the phase diagram, and (i) Poincare map with $C = 0.4$.

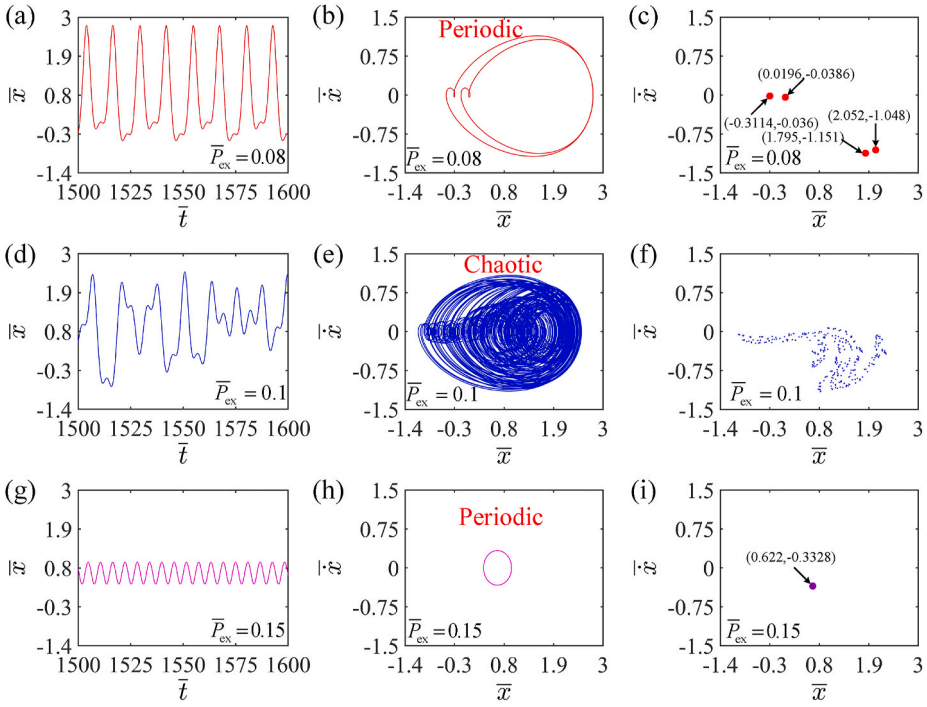

Fig. 15. Self-sustained floating behaviors of LCE balloon with different dimensionless external pressures. (a) Time-history curve, (b) Limit cycle in the phase diagram, and (c) Poincare map with $\overline{P}_{ex} = 0.08$;(d) Time-history curve, (e) Attractor in the phase diagram, and (f) Poincare map with $\overline{P}_{ex} = 0.1$;(g) Time-history curve, (h) Limit cycle in the phase diagram, and (i) Poincare map with $\overline{P}_{ex} = 0.15$.

with the increasing external pressure. Fig. 15(c), (f) and (i) show that the number of points on the Poincare diagram varies from single to multiple, and then to single with the increasing external pressure. The Poincare map in Fig. 15(f) suggests that chaotic phenomenon of the self-exited floating system emerges at $\overline{P}_{ex} = 0.1$. It is summarized by numerical calculations that when the external pressure is in the interval of 0.099–0.102, chaotic phenomenon of the self-sustained floating will appear. For too small or too large external pressure, the system will not display chaotic phenomenon. Similarly, this is because that the spring force or buoyancy acts dominant for too small or too large external pressure, which causes the LCE balloon to self-float near the low or high potential wells.

5.6. *Effect of beating damping coefficient*

This section mainly presents a discussion on the deformation beating damping coefficient affecting chaotic phenomena of self-sustained floating. Hereon, the time-history curve, phase diagram and Poincare map of the floating behaviors of the LCE balloon for $\overline{\beta}$ are portrayed in Fig. 16, in which the other dimensionless parameters are selected as follows: $\overline{\rho}_a = 0.6$, $\overline{\rho}_L = 2.5$, $\overline{k} = 0.05$, $\overline{\alpha} = 0.02$, $\overline{I}_0 = 0.2$, $C = 0.3$, $\overline{n} = 0.5$, $\overline{V} = 0.6$ and $\overline{P}_{ex} = 0.1$. The value of beating damping coefficient is found to influence the appearance of chaotic phenomenon. Summarized from the comparison among Fig. 16(a), (d) and (g), with the increase of deformation beating damping coefficient, the time-history curve undergoes a variation from order to disorder, and then to order again. Whereas, the floating amplitude exhibits a decline trend since the increase of beating damping coefficient restrains the change of buoyancy. By comparing Fig. 16(b), (e) and (h), the phase diagram displays a change from simple to complex, and then to simple again with the increase of deformation damping coefficient. In the comparison of Fig. 16(c), (f) and (i), as the beating damping coefficient increases, a number variation from single to multiple, and then to single happens to the points on the Poincare diagram. The Poincare map in Fig. 16(f) shows that chaotic phenomenon of the self-exited floating system takes place at $\overline{\beta} = 0.08$. Concluded from the numerical calculations, chaotic phenomenon of the self-sustained floating will take place when the deformation damping coefficient of LCE balloon is in the range of 0.06–0.1. For too small or too large deformation damping coefficient, the system will not appear chaotic phenomenon. Similarly, the reason for this phenomenon is that for too small or too large deformation damping coefficient, buoyancy or spring force plays a leading role, thus the LCE balloon exhibits a final self-floating near the low or high potential wells.

5.7. *Effect of the amount of substance*

This section mainly discusses the effect of amount of substance on chaotic phenomena of self-sustained floating. Hereon, Fig. 17 gives the time-history curve, phase diagram and Poincare map of the floating behaviors of the LCE balloon for different $\overline{n}$, where the other dimensionless parameters are selected as follows: $\overline{\rho}_a = 0.6$, $\overline{\rho}_L = 2.5$, $\overline{k} = 0.05$, $\overline{\alpha} = 0.02$, $\overline{\beta} = 0.1$, $\overline{I}_0 = 0.2$, $C = 0.3$, $\overline{V} = 0.6$

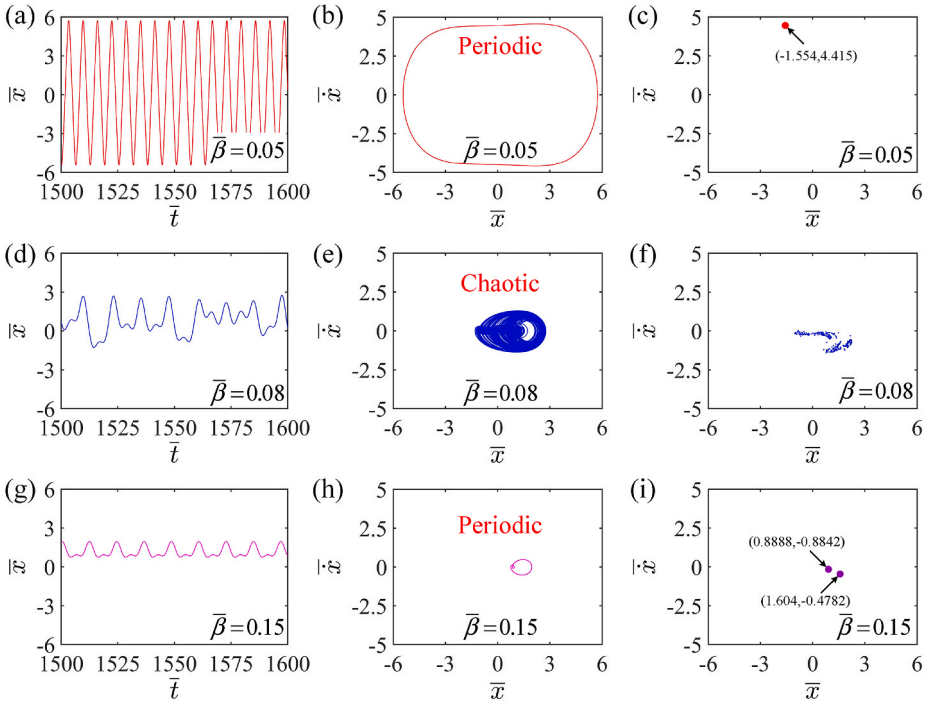

Fig. 16. Self-sustained floating behaviors of LCE balloon with different dimensionless beating damping coefficients. (a) Time-history curve, (b) Limit cycle in the phase diagram, and (c) Poincare map with $\overline{\beta} = 0.05$;(d) Time-history curve, (e) Attractor in the phase diagram, and (f) Poincare map with $\overline{\beta} = 0.08$;(g) Time-history curve, (h) Limit cycle in the phase diagram, and (i) Poincare map with $\overline{\beta} = 0.15$.

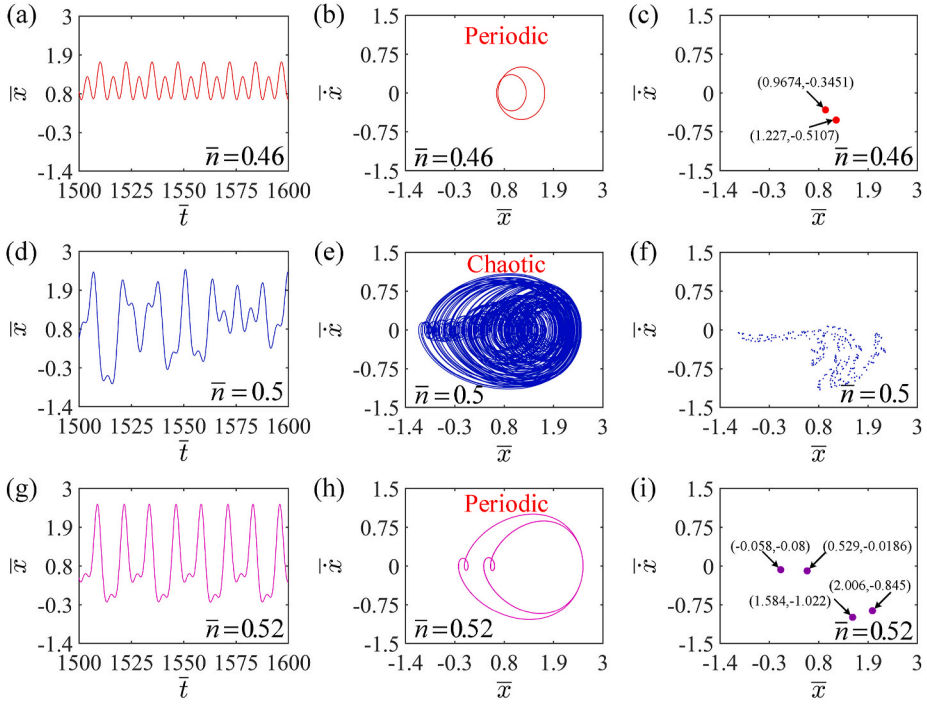

Fig. 17. Self-sustained floating behaviors of LCE balloon with different dimensionless amounts of substance. (a) Time-history curve, (b) Limit cycle in the phase diagram, and (c) Poincare map with $\overline{n} = 0.46$;(d) Time-history curve, (e) Attractor in the phase diagram, and (f) Poincare map with $\overline{n} = 0.5$;(g) Time-history curve, (h) Limit cycle in the phase diagram, and (i) Poincare map with $\overline{n} = 0.52$.

and $\overline{P}_{ex} = 0.1$. It can be intuitively seen from Fig. 17 that the value of amount of substance has an impact on the appearance of chaotic phenomenon. Through the comparison among Fig. 17(a), (d) and (g), it can be found that the time-history curve changes from order to disorder, and then to order again as the amount of substance increases. In addition, the floating amplitude is enlarged as a result of the increasing amount of substance promoting the change of buoyancy. Similarly, the comparison of Fig. 17(b), (e) and (h) figures out that the phase diagram changes from simple to complex, and then to simple again with the increasing amount of substance. Fig. 17(c), (f) and (i) show that the number of points on the Poincare diagram alters from single to multiple, and then to single with the increasing amount of substance. The Poincare map in Fig. 17(f) presents that chaotic phenomenon of the self-exited floating system appears at $\overline{n} = 0.5$. Summarized from the numerical calculations, when the amount of substance of ideal gas is between 0.496 and 0.511, chaotic phenomenon of the self-sustained floating will occur. For too small or too large amount of substance, the system will not appear chaotic phenomenon. This phenomenon can be understood by analogy with the influence of external pressure. For too small or too large amount of substance, spring force or buoyancy is dominant, thus chaotic phenomenon will not occur.

5.8. *Effect of the LCE mass density*

The effect of LCE mass density on chaotic phenomena of self-sustained floating is discussed in current section. Hereon, the time-history curve, phase diagram and Poincare map of the floating behaviors of the LCE balloon for different $\overline{\rho}_L$ are portrayed in Fig. 18, in which the other dimensionless parameters are selected as follows: $\overline{\rho}_a = 0.6$, $\overline{k} = 0.05$, $\overline{\alpha} = 0.02$, $\overline{\beta} = 0.1$, $\overline{I}_0 = 0.2$, $C = 0.3$, $\overline{n} = 0.5$, $\overline{V} = 0.6$ and $\overline{P}_{ex} = 0.1$. Clearly seen from Fig. 18 that the value of LCE density has an influence on the appearance of chaotic phenomenon. By comparing Fig. 18(a), (d) and (g), it can be summarized that the time-history curve follows the law of change from order to disorder to order again with the increase of LCE mass density. Furthermore, the floating amplitude of the LCE balloon exhibits an increasing trend with the increase of LCE density, and the floating position moves down due to the increasing gravity. The comparison among Fig. 18(b), (e) and (h) reveals that the phase diagrams change from simple to complex to simple again with the increase of LCE density. By comparing Fig. 18(c), (f) and (i), the points number on the Poincare diagram is found to change from single to multiple to single again with the increase of LCE density. The Poincare map in Fig. 18(f) demonstrates that chaotic phenomenon of the self-exited floating system emerges at $\overline{\rho}_L = 3.3$. It is found by numerical calculations that chaotic phenomenon will come into being when the dimensionless LCE density parameter locates between 2.5 and 3.5. For too small or too large LCE density, the system will not appear chaotic phenomenon. This phenomenon can be understood by analogy with the influence of air mass density. For too small or too large LCE mass density, buoyancy or spring force acts dominant, thus chaotic phenomenon will not come into being.

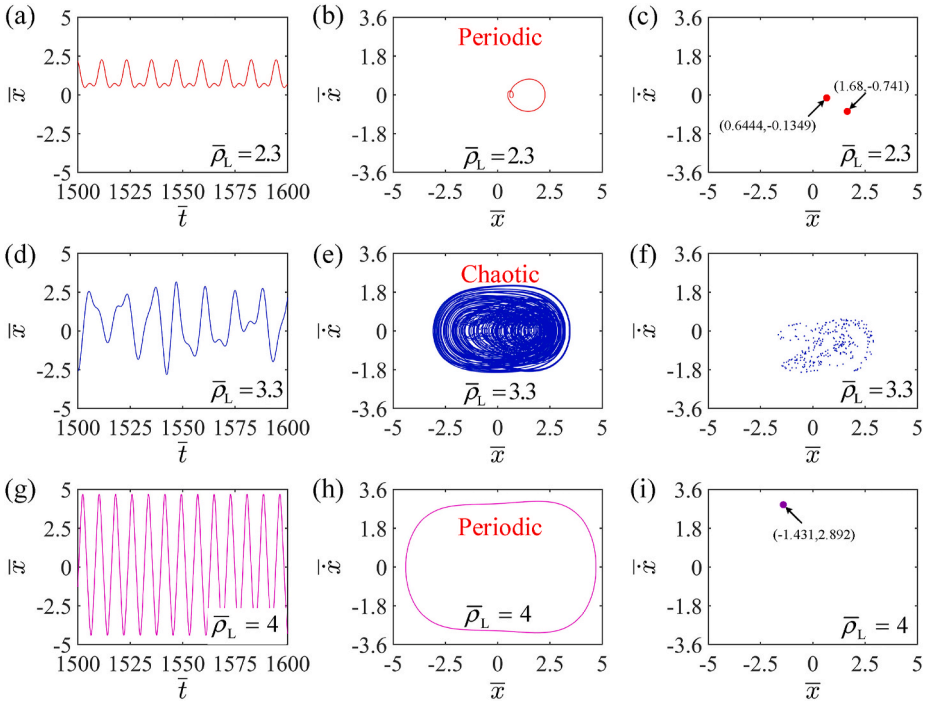

Fig. 18. Self-sustained floating behaviors of LCE balloon with different dimensionless LCE mass densities. (a) Time-history curve, (b) Limit cycle in the phase diagram, and (c) Poincare map with $\overline{\rho}_L = 2.3$;(d) Time-history curve, (e) Attractor in the phase diagram, and (f) Poincare map with $\overline{\rho}_L = 3.3$;(g) Time-history curve, (h) Limit cycle in the phase diagram, and (i) Poincare map with $\overline{\rho}_L = 4$.

5.9. Effect of the LCE volume

This section mainly focuses on the effect of LCE volume on chaotic phenomena of self-sustained floating. Hereon, the time-history curve, phase diagram and Poincare map of the floating behaviors of the LCE balloon for different $\overline{V}$ are portrayed in Fig. 19, where the other dimensionless parameters are selected as follows: $\overline{\rho}_a = 0.6, \overline{\rho}_L = 2.5, \overline{k} = 0.05, \overline{\alpha} = 0.02, \overline{\beta} = 0.1, \overline{I}_0 = 0.2, C = 0.3, \overline{n} = 0.5$ and $\overline{P}_{ex} = 0.1$. The value of LCE volume is found to have effect on the occurrence of chaotic phenomenon. Conclusions can be drawn from the comparison of Fig. 19(a), (d) and (g) that as the LCE volume experiences an increase, the time-history curve changes from order to disorder, and then to order again. A similar comparison is conducted to Fig. 19(b), (e) and (h), the phase diagram is observed to display a variation from simple to complex, and then to simple again with the increasing LCE volume. It can be also concluded by comparing Fig. 19(c), (f) and (i) that the points on the Poincare diagram change from single to multiple, and then to single with the increasing LCE volume. The Poincare map in Fig. 19(f) shows that chaotic phenomenon of the self-sustained floating system appears at $\overline{V} = 0.6$. Summary could be obtained from numerical calculations that chaotic phenomenon will appear when the dimensionless LCE volume parameter is in the interval of 0.598–0.613. For too small or too large LCE volume, the chaotic phenomenon will not take place. This phenomenon can be understood by analogy with the influence of the amount of substance. For too small or too large LCE volume, buoyancy or spring force displays a cardinal role, thus chaotic phenomenon will not take place.

6. Conclusions

Self-sustained chaotic system has the capability to maintain its own motion through directly absorbing energy from the steady external environment, and has shown extensive application potential in energy harvesters, self-cleaning, biomimetic robots, encrypted communication and other fields. In current paper, we propose a novel light-powered chaotic self-floating system, which is comprised by a nonlinear spring and a LCE balloon. The proposed system is capable of self-beating under steady illumination due to self-shading effect. Combined the Newtonian dynamics with dynamic LCE model, the corresponding theoretical model is formulated. Numerical calculations show that the periodic self-floating of LCE balloon can occur under steady illumination, which originates from the light-powered self-beating of LCE balloon with shading coating. The self-floating is maintained by compensating the damping energy dissipation through the net work done by the buoyancy of LCE balloon. Furthermore, the chaotic self-floating is presented to be developed from the periodic self-floating through period-doubling bifurcation. Besides, different system parameters involving light intensity, LCE contraction coefficient, air density, LCE density and volume, stiffness coefficient of the spring, external pressure, motion and deformation damping coefficient, will affect the amplitude, equilibrium position and chaotic behavior of the new self-sustained chaotic system. It is expected that someone can realize this experimentally in the future, and the power spectrum measured

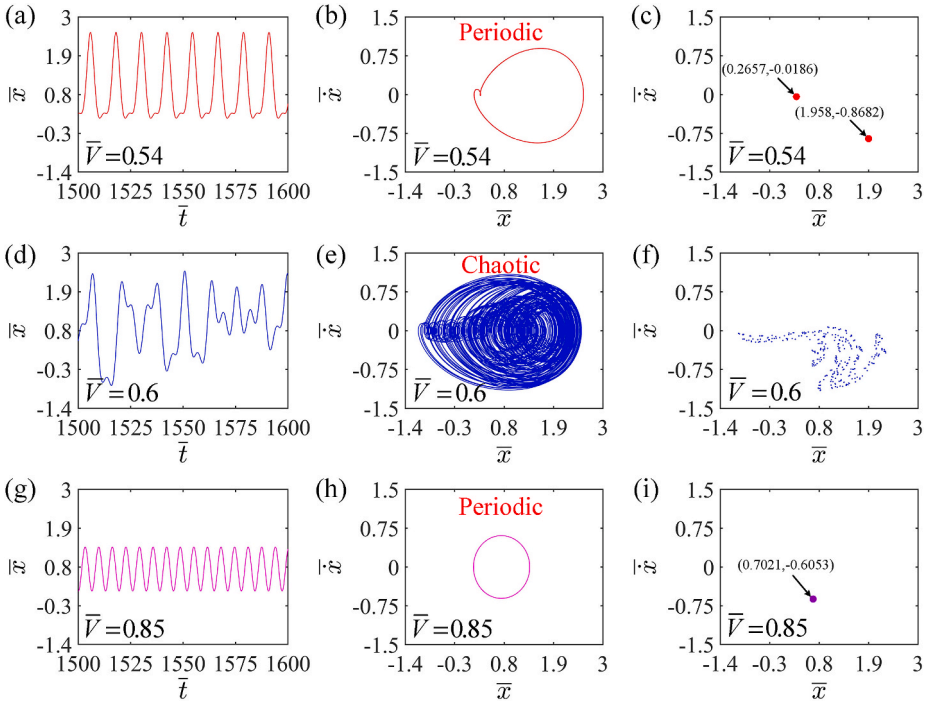

Fig. 19. Self-sustained floating behaviors of LCE balloon with different dimensionless LCE volumes. (a) Time-history curve, (b) Limit cycle in the phase diagram, and (c) Poincare map with $\overline{V} = 0.54$;(d) Time-history curve, (e) Attractor in the phase diagram, and (f) Poincare map with $\overline{V} = 0.6$; (g) Time-history curve, (h) Limit cycle in the phase diagram, and (i) Poincare map with $\overline{V} = 0.85$.

experimentally can be considered to be compared with the present numerical results. In addition, the chaotic self-floating system of current study may inspire the design of other chaotic self-sustained motion based on stimuli-responsive materials, and have guiding significance for energy harvesters, self-cleaning, biomimetic robots, encrypted communication and other applications.

Author contribution statement

Peibao Xu, Kai Li: Conceived and designed the theoretical investigations; Analyzed and interpreted the data; Wrote the paper.

Haiyang Wu: Performed the theoretical investigations; Analyzed and interpreted the data; Contributed reagents, materials, analysis tools or data.

Yuntong Dai: Analyzed and interpreted the data; Wrote the paper.

Funding statement

Professor Kai Li was supported by University Natural Science Research Project of Anhui Province [2022AH020029]; National Natural Science Foundation of China [12172001]; Anhui Provincial Natural Science Foundation [2208085Y01].

Yuntong Dai was supported by Anhui Provincial Natural Science Foundation [2008085QA23].

Peibao Xu was supported by Anhui Provincial Natural Science Foundation [2008085QA50]; Key Project of University Natural Science Research Project of Anhui Province [KJ2020A0452].

Data availability statement

No data was used for the research described in the article.

Declaration of interest's statement

The authors declare no conflict of interest.

References

[1] M.H. Li, P. Keller, B. Li, X. Wang, M. Brunet, Light-driven side-on nematic elastomer actuators, Adv. Mater. 15 (2003) 569–572.
[2] X. Wang, C.F. Tan, K.H. Chan, X. Lu, L. Zhu, S. Kim, G.W. Ho, In-built thermo-mechanical cooperative feedback mechanism for self-propelled multimodal locomotion and electricity generation, Nat. Commun. 9 (2018) 3438.
[3] S. Nocentini, C. Parmeggiani, D. Martella, D.S. Wiersma, Optically driven soft micro robotics, Adv. Opt. Mater. 6 (2018), 1800207.
[4] F. Ge, R. Yang, X. Tong, F. Camerel, Y. Zhao, A multifunctional dyedoped liquid crystal polymer actuator: light-guided transportation, turning in locomotion, and autonomous motion, Angew. Chem., Int. Ed. 57 (2018) 11758–11763.
[5] C. Du, Q. Cheng, K. Li, Y. Yu, A light-powered liquid crystal elastomer spring oscillator with self-shading coatings, Polymers 14 (2022) 1525.
[6] J. Zhao, P. Xu, Y. Yu, K. Li, Controllable vibration of liquid crystal elastomer beams under periodic illumination, Int. J. Mech. Sci. 170 (2022), 105366.
[7] H. Zeng, M. Lahikainen, L. Liu, Z. Ahmed, O.M. Wani, M. Wang, A. Priimagi, Light-fuelled freestyle self-oscillators, Nat. Commun. 10 (2019) 5057.
[8] K. Korner, A.S. Kuenstler, R.C. Hayward, B. Audoly, K. Bhattacharya, A nonlinear beam model of photomotile structures, Proc. Natl. Acad. Sci. U.S.A. 117 (2020) 9762–9770.
[9] D. Martella, S.C. Nocentini, C. Parmeggiani, D.S. Wiersma, Self-regulating capabilities in photonic robotics, Adv Mater Technol 4 (2019), 1800571.
[10] B. Shin, J. Ha, M. Lee, K. Park, G.H. Park, T.H. Choi, K.J. Cho, H.Y. Kim, Hygrobot: a self-locomotive ratcheted actuator powered by environmental humidity, Sci Robot 3 (2018) eaar2629.
[11] P. Rothemund, A. Ainla, L. Belding, D.J. Preston, S. Kurihara, Z. Suo, G.M. Whitesides, A soft bistable valve for autonomous control of soft actuators, Sci Robot 3 (2018), eaar7986.
[12] G. Vantomme, A.H. Gelebart, D.J. Broer, E.W. Meijer, A four-blade light-driven plastic mill based on hydrazone liquid-crystal networks, Tetrahedron 73 (2017) 4963–4967.
[13] Z. Liu, M. Qi, Y. Zhu, D. Huang, X. Zhang, L. Lin, X. Yan, Mechanical response of the isolated cantilever with a floating potential in steady electrostatic field, Int. J. Mech. Sci. 161 (2019), 105066.
[14] Y. Kageyama, T. Ikegami, S. Satonaga, K. Obara, H. Sato, S. Takeda, Light-driven flipping of azobenzene assemblies-sparse crystal structures and responsive behavior to polarized light, Chem. Eur J. 26 (2020) 10759–10768.
[15] B. Liao, H. Zang, M. Chen, Y. Wang, X. Lang, N. Zhu, Z. Yang, Y. Yi, Soft rod-climbing robot inspired by winding locomotion of snake, Soft Robot. 7 (2020) 500–511.
[16] T.J. White, N.V. Tabiryan, S.V. Serak, U.A. Hrozhyk, V.P. Tondiglia, H. Koerner, R.A. Vaia, T.J. Bunning, A high frequency photodriven polymer oscillator, Soft Matter 4 (2008) 1796–1798.
[17] C. Ahn, K. Li, S. Cai, Light or thermally powered autonomous rolling of an elastomer rod, ACS Appl. Mater. Interfaces 10 (2018) 25689–25696.
[18] X. Lu, H. Zhang, G. Fei, B. Yu, X. Tong, H. Xia, Y. Zhao, Liquid-crystalline dynamic networks doped with gold nanorods showing enhanced photocontrol of actuation, Adv. Mater. 30 (2018), 1706597.
[19] Y. Cheng, H. Lu, X. Lee, H. Zeng, A. Priimagi, Kirigami-based light-induced shape-morphing and locomotion, Adv. Mater. 32 (2019), 1906233.
[20] S. Chun, C. Pang, S.B. Cho, A micropillar-assisted versatile strategy for highly sensitive and efficient triboelectric energy generation under in-plane stimuli, Adv. Mater. 32 (2020), 1905539.
[21] R. Tang, Z. Liu, D. Xu, J. Liu, L. Yu, H. Yu, Optical pendulum generator based on photomechanical liquid-crystalline actuators, ACS Appl. Mater. Interfaces 7 (2015) 8393–8397.
[22] D. Zhao, Y. Liu, A prototype for light-electric harvester based on light sensitive liquid crystal elastomer cantilever, Energy 198 (2020), 117351.
[23] L. Yang, L. Chang, Y. Hu, M. Huang, Q. Ji, P. Lu, J. Liu, W. Chen, Y. Wu, An autonomous soft actuator with light-driven self-sustained wavelike oscillation for phototactic self-locomotion and power generation, Adv. Funct. Mater. 30 (2020), 1908842.
[24] M. Yamada, M. Kondo, J.I. Mamiya, Photomobile polymer materials: towards light-driven plastic motors, Angew. Chem. Int. Ed. 47 (2008) 4986–4988.
[25] A. Shastri, L. McGregor, Y. Liu, V. Harris, H. Nan, M. Mujica, Y. Vasquez, A. Bhattacharya, Y. Ma, M. Aizenberg, O. Kuksenok, A. Balazs, J. Aizenberg, X. He, An aptamer-functionalized chemomechanically modulated biomolecule catch-and-release system, Nat. Chem. 7 (2015) 447–454.
[26] M.F. Eggl, P.J. Schmid, Mixing by stirring: optimizing shapes and strategies, Phys Rev Fluids 7 (2022), 073904.
[27] T. White, D. Broer, Programmable and adaptive mechanics with liquid crystal polymer networks and elastomers, Nat. Mater. 14 (2015) 1087–1098.

[28] X. He, M. Aizenberg, O. Kuksenok, L. Zarzar, S. Ankita, A. Balazs, J. Aizenberg, Synthetic homeostatic materials with chemo-mechano-chemical self-regulation, Nature 487 (2012) 214–218.
[29] S. Kinoshita, Introduction to nonequilibrium phenomena, in: Pattern Formations and Oscillatory Phenomena. Amsterdam, 2013, pp. 1–59.
[30] A. Chakrabarti, G.P. Choi, L. Mahadevan, Self-excited motions of volatile drops on swellable sheets, Phys. Rev. Lett. 124 (2020), 258002.
[31] M. Lahikainen, H. Zeng, A. Priimagi, Reconfigurable photoactuator through synergistic use of photochemical and photothermal effects, Nat. Commun. 9 (2018) 4148.
[32] P. Palffy-Muhoray, Liquid crystal elastomers and light. Liquid crystal elastomers: materials and applications, Adv. Polym. Sci. 250 (2012) 95–118.
[33] M. Camacho-Lopez, H. Finkelmann, P. Palffy-Muhoray, M. Shelley, Fast liquid-crystal elastomer swims into the dark, Nat. Mater. 3 (2004) 307–310.
[34] H. Koibuchi, Bending of thin liquid crystal elastomer under irradiation of visible light: finsler geometry modeling, Polymers 10 (2018) 757.
[35] V.V. Yashin, A.C. Balazs, Pattern formation and shape changes in self-oscillating polymer gels, Science 314 (2006) 798–801.
[36] J. Zhang, Q. Huang, J. Du, Recent advances in magnetic hydrogels, Polym. Int. 65 (2016) 1365–1372.
[37] J. Boissonade, P. De Kepper, Multiple types of spatio-temporal oscillations induced by differential diffusion in the Landolt reaction, Phys. Chem. Chem. Phys. 13 (2011) 4132–4137.
[38] K. Li, P.Y. Wu, S.Q. Cai, Chemomechanical oscillations in a responsive gel induced by an autocatalytic reaction, J. Appl. Phys. 116 (2014), 043523.
[39] K. Li, Z. Chen, Z. Wang, S.Q. Cai, Self-sustained eversion or inversion of a thermally responsive torus, Phys. Rev. E 103 (2021), 033004.
[40] Y.H. Na, Y. Aburaya, H. Orihara, K. Hiraoka, Measurement of electrically induced shear strain in a chiral smectic liquid-crystal elastomer, Phys. Rev. E 83 (2011), 061709.
[41] J.M. Haber, A. Sanchez-Ferrer, A.M. Mihut, H. Dietsch, A.M. Hirt, R. Mezzenga, Liquid-crystalline elastomer-nanoparticle hybrids with reversible switch of magnetic memory, Adv. Mater. 25 (2013) 1787–1791.
[42] X. Liang, Z. Chen, L. Zhu, K. Li, Light-powered self-excited oscillation of a liquid crystal elastomer pendulum, Mech. Syst. Signal Process. 163 (2022), 108140.
[43] A.S. Kuenstler, Y. Chen, P. Bui, H. Kim, A. DeSimone, L. Jin, R.C. Hayward, Blueprinting photothermal shape-morphing of liquid crystal elastomers, Adv. Mater. 32 (2020), 2000609.
[44] Q. Cheng, X. Liang, K. Li, Light-powered self-excited motion of a liquid crystal elastomer rotator, Nonlinear Dynn 103 (2021) 2437–2449.
[45] Y.C. Cheng, H.C. Lu, X. Lee, H. Zeng, A. Priimagi, Kirigami-based light-induced shape-morphing and locomotion, Adv. Mater. 32 (2020), 1906233.
[46] Y. Kim, J. van den Berg, A.J. Crosby, Autonomous snapping and jumping polymer gels, Nat. Mater. 20 (2021) 1695–1701.
[47] G. Graeber, K. Regulagadda, P. Hodel, C. Küttel, D. Landolf, T.M. Schutzius, D. Poulikakos, Leidenfrost droplet trampolining, Nat. Commun. 12 (2021) 1727.
[48] P. Xu, J. Jin, K. Li, Light-powered self-excited bouncing of a liquid crystal elastomer ball, Int. J. Mech. Sci. 208 (2021), 106686.
[49] A. Gelebart, D. Jan Mulder, M. Varga, A. Konya, G. Vantomme, E.W. Meijer, R. Selinger, D. Broer, Making waves in a photoactive polymer film, Nature 546 (2017) 632–636.
[50] T. Xu, D. Pei, S. Yu, X. Zhang, M. Yi, C. Li, Design of mxene composites with biomimetic rapid and self-oscillating actuation under ambient circumstances, ACS Appl. Mater. Interfaces 13 (2021) 31978–319853.
[51] M.P.D. Cunha, A.R. Peeketi, A. Ramgopal, R.K. Annabattula, A.P.H.J. Schenning, Light-driven continual oscillatory rocking of a polymer film, Chemistry Open 9 (2020) 1149–11525.
[52] K. Li, Z. Chen, P. Xu, Light-propelled self-sustained swimming of a liquid crystal elastomer torus at low Reynolds number, Int. J. Mech. Sci. 219 (2022), 1071287.
[53] K. Li, X. Su, S. Cai, Self-sustained rolling of a thermally responsive rod on a hot surface, Extreme Mech Lett 42 (2021), 101116.
[54] Q. Cheng, L. Zhou, C. Du, K. Li, A light-fueled self-oscillating liquid crystal elastomer balloon with self-shading effect, Chaos, Solit. Fractals 155 (2022), 11646.
[55] K. Kumar, C. Knie, D. Bléger, M.A. Peletier, H. Friedrich, S. Hecht, D. Broer, M.G. Debije, A. Schening, A chaotic self-oscillating sunlight-driven polymer actuator, Nat. Commun. 7 (2016), 11975.
[56] H. Yu, T. Ikeda, Photocontrollable liquid-crystalline actuators, Adv. Mater. 23 (2011) 2149–2180.
[57] C. Li, Y. Liu, X. Huang, H. Jiang, Direct sun-driven artificial heliotropism for solar energy harvesting based on a photo-thermomechanical liquid-crystal elastomer nanocomposite, Adv. Funct. Mater. 22 (2022) 5166–5174.
[58] A. Bobtsov, A. Pyrkin, N. Nikolaev, O. Slita, Adaptive observer design for a chaotic Duffing system, Int J Robust Nonlin 19 (2009) 829–841.
[59] S. Liao, X. Li, Y. Yang, Three-body problem - from Newton to supercomputer plus machine learning, N. Astron. 96 (2022), 101850.
[60] C. Li, G. Luo, C. Li, A parallel image encryption algorithm based on chaotic Duffing oscillators, Multimed. Tool. Appl. 77 (2018) 19193–19208.
[61] Q. Cheng, W. Cheng, Y. Dai, K. Li, Self-oscillating floating of a spherical liquid crystal elastomer balloon under steady illumination, Int. J. Mech. Sci. 241 (2023), 107985.
[62] T. Nägele, R. Hoche, W. Zinth, J. Wachtveitl, Femtosecond photoisomerization of cis-azobenzene, Chem. Phys. Lett. 272 (1997) 489–495.
[63] W. Cheng, Q. Cheng, C. Du, Y. Dai, K. Li, Beating of a spherical liquid crystal elastomer balloon under periodic illumination, Micromachines -Basel 13 (5) (2022) 769.
[64] Jakob L. Laugesen, Erik Mosekilde, Zhanybai T. Zhusubaliyev, Bifurcation structure of the C-type period-doubling transition, Physica D 241 (2012) 488–496.
[65] R. Yanushkevichius, On ε-independence of Sample Mean and Sample Variance. Stability Problems for Stochastic Models, Springer Berlin Heidelberg, 1987, pp. 207–223.